

Dalton Transactions

Accepted Manuscript



This is an *Accepted Manuscript*, which has been through the Royal Society of Chemistry peer review process and has been accepted for publication.

Accepted Manuscripts are published online shortly after acceptance, before technical editing, formatting and proof reading. Using this free service, authors can make their results available to the community, in citable form, before we publish the edited article. We will replace this *Accepted Manuscript* with the edited and formatted *Advance Article* as soon as it is available.

You can find more information about *Accepted Manuscripts* in the [Information for Authors](#).

Please note that technical editing may introduce minor changes to the text and/or graphics, which may alter content. The journal's standard [Terms & Conditions](#) and the [Ethical guidelines](#) still apply. In no event shall the Royal Society of Chemistry be held responsible for any errors or omissions in this *Accepted Manuscript* or any consequences arising from the use of any information it contains.

1 **Composition-solubility-structure relationships in calcium (alkali)**
2 **aluminosilicate hydrate (C-(N,K-)A-S-H)**

3
4 Rupert J. Myers ^{1,2,a}, Emilie L'Hôpital ^{2,b}, John L. Provis ^{1,c}, Barbara Lothenbach ^{2*}

5
6 ¹ Department of Materials Science and Engineering, University of Sheffield, S1 3JD,
7 Sheffield, United Kingdom

8
9 ² Laboratory for Concrete and Construction Chemistry, EMPA, Dübendorf, 8600, Switzerland

10
11 * Corresponding author. Email Barbara.Lothenbach@empa.ch

12 ^a rupert.myers@gmail.com. ^b lhospital.emilie@gmail.com. ^c j.provis@sheffield.ac.uk.

13
14
15 **Abstract**

16
17 The interplay between the solubility, structure and chemical composition of calcium (alkali)
18 aluminosilicate hydrate (C-(N,K-)A-S-H) equilibrated at 50°C is investigated in this paper.
19 The tobermorite-like C-(N,K-)A-S-H products are more crystalline in the presence of alkalis
20 and generally have larger basal spacings at lower Ca/Si ratios. Both Na and K are
21 incorporated into the interlayer space of the C-(N,K-)A-S-H phases, with more alkali uptake
22 observed at higher alkali and lower Ca content. No relationship between Al and alkali uptake
23 is identified at the Al concentrations investigated ($\text{Al/Si} \leq 0.1$). More stable C-(N,K-)A-S-H
24 is formed at higher alkali content, but this factor is only significant in some samples with
25 Ca/Si ratios ≤ 1 . Shorter chain lengths are formed at higher alkali and Ca content, and cross-

26 linking between (alumino)silicate chains in the tobermorite-like structure is greatly promoted
27 by increasing alkali and Al concentrations. The calculated solubility products do not depend
28 greatly on the mean chain length in C-(N,K-)A-S-H at a constant Ca/(Al+Si) ratio, or the
29 Al/Si ratio in C-(N,K-)A-S-H. These results are important for understanding the chemical
30 stability of C-(N,K-)A-S-H, which is a key phase formed in the majority of cements and
31 concretes used worldwide.

32

33 **1. Introduction**

34

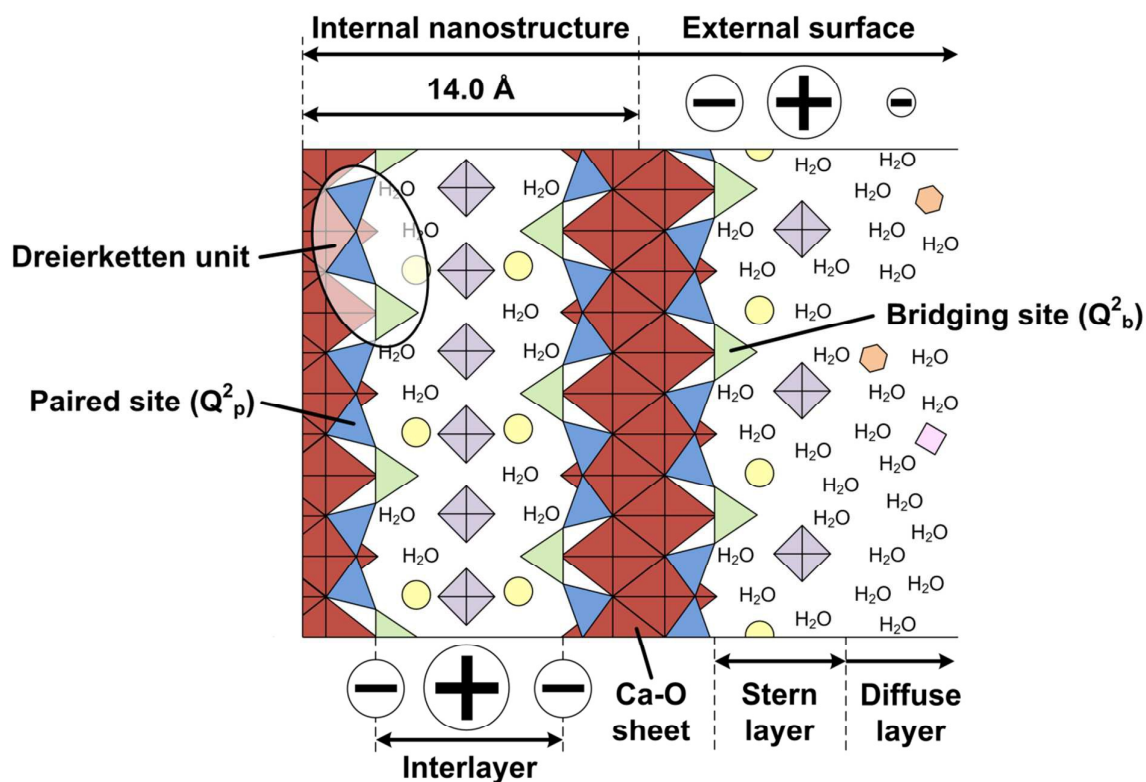
35 The alkali concentration in cement-based materials varies greatly as a function of the cement
36 formulation and type: Portland cement (PC) typically contains up to 1 wt.% alkali (mainly K)
37 oxide equivalent;¹ fly ash, a common supplementary cementitious material (SCM), generally
38 contains >1 wt.% alkali (Na + K) oxide equivalent;² and alkali-activated cementitious
39 materials typically involve the use of highly concentrated Na-based solutions (up to or
40 exceeding 5 M).³ The elevated pH environment that prevails in hydrated cement-based
41 materials (pH > 13) provides the crucial function of steel passivation in reinforced concrete.
42 The alkali concentration in cement-based materials also plays an important role in the
43 dissolution of cementitious precursors,^{4, 5} deterioration of concrete due to alkali-silica
44 reactions,^{6, 7} and in modifying the chemical composition, structure and solubility of reaction
45 products formed during setting and hardening.⁸⁻¹¹

46

47 The main reaction product in hydrated Portland cement (PC) materials is calcium (alkali)
48 silicate hydrate (C-(N,K-)S-H^a) with a structure analogous to the natural mineral

^a Na and K are included in this abbreviation because these are typically the most concentrated alkali elements in cement-based materials. Cement chemistry notation is also used throughout the paper: C = CaO; S = SiO₂; A = Al₂O₃; N = Na₂O; K = K₂O; and H = H₂O.

49 tobermorite, usually with $\text{Ca}/(\text{Al}+\text{Si}) \geq 1.5$, and sometimes with minor Al substitution up to
50 an Al/Si ratio not exceeding 0.1.¹² This phase contains silicate (or aluminosilicate if Al is
51 present) chains in dreierketten type arrangements, flanked on either side by a Ca-O sheet and
52 an interlayer region (Figure 1).¹³ These aluminosilicate chains can cross-link to form Q³-type
53 structures,¹⁴ and if present, Al is bound in bridging sites with a strong preference over the
54 paired sites.¹⁵ Al is also thought to be incorporated in C-(N,K-)A-S-H in five- and six-fold
55 coordination, *e.g.* in the interlayer (Figure 1), although no consensus exists regarding the
56 location of octahedral Al in this phase.¹⁶⁻¹⁸ The Ca-O sheets, interlayer regions and
57 (alumino)silicate chains are thought to stack together such that the chain structures form the
58 external surfaces.¹⁹
59



60
61
62
63
64
65
66
67
68
69
70
71
72
73
74
75

Figure 1. Schematic representation of infinite chain length non-cross-linked C-(N,K-)A-S-H as a structural analogue of 14 Å tobermorite,²⁰ with stacked layers to show alkali species adsorbed on the external surface and in the interlayer region of this phase. The red diamonds are CaO polyhedra in the Ca-O sheet, and the blue and green triangles are tetrahedral aluminate or silicate units in paired and bridging sites respectively, within the dreierketten chains. The yellow circles and large purple squares represent positively-charged species that charge-neutralise the bridging sites and the rest of the layered structure respectively (typically H⁺, Ca²⁺, alkali cations such as K⁺ or Na⁺, and/or dissolved aluminium). The orange hexagons are diffuse layer anions (*e.g.* OH⁻ and Cl⁻) that compensate the excess positive charge supplied by adsorbed cations.¹⁹ The small pink square is an additional diffuse layer cation (*e.g.* Ca²⁺, Na⁺). The positive and negative symbols represent the local distribution of charge in the structure. The size, number and location of the symbols are schematic rather than crystallographically exact, and different types of hydrated alkali complexes are not distinguished.

76 The essentially aluminium-free C-(N,K-)S-H formed during plain Portland cement hydration
77 can incorporate a significant content of alkalis (up to 20% of the amount of Na or K added
78 ²¹), which decreases as a direct function of the Ca/Si ratio.²¹ A good understanding of C-
79 (N,K-)S-H solubility currently exists up to bulk Na concentrations of 0.8 M NaOH,^{8, 9, 21-24}
80 which represents the pH range relevant to most cement-based materials (pH ≤ 13.5), but
81 fewer solubility data for this phase are available for K-containing materials in the

82 corresponding composition range.^{21, 22, 25, 26} These data are essential in understanding the
83 long-term stability of C-(N,K-)S-H and in the development of thermodynamic models for this
84 phase, enabling simulation of the chemistry of cement-based materials in service.^{27, 28}

85

86 However, many modern blended cements contain more Al and less Ca than plain PC. The
87 main hydrate in binders produced from these materials is a calcium (alkali) aluminosilicate
88 hydrate (C-(N,K-)A-S-H^b) with typical molar ratios of $\text{Ca}/(\text{Al}+\text{Si}) \leq 1.5$ and $\text{Al}/\text{Si} > 0.1$.^{29, 30}

89 C-(N,K-)A-S-H phases are also major reaction products in ~2000 year old Roman cements.³¹

90 Incorporation of alkali species into the interlayer region and on external surfaces of C-(N,K-
91)A-S-H is believed to occur via a charge-compensation mechanism (Figure 1),^{11, 19, 32, 33} with

92 less associated alkalis at higher Ca/Si ratios (similar to C-(N,K-)S-H),³⁴ although no

93 consensus exists regarding the exact mechanism of alkali uptake in this phase. This is

94 corroborated by the large variation in existing results reported for Na and K uptake as a

95 function of Al content in C-(N,K-)A-S-H: direct correlations,^{33, 34} an inverse correlation,²⁵

96 and independent relationships^{6, 11, 35} between these two parameters have been reported. There

97 is also a lack of consensus on the selectivity of C-(N,K-)A-S-H structures between Na or K

98 species, with existing publications reporting either no significant difference between uptake

99 of these two alkali types,^{8, 21, 25, 34} or some degree of selectivity for K over Na.¹¹ This clearly

100 demonstrates a need for additional studies to clarify the relationships between the uptake of

101 Na, K and Al in C-(N,K-)A-S-H.

102

103 The solubility of Al-containing C-(N,K-)A-S-H is poorly understood relative to that of C-

104 (N,K-)S-H, although recent results¹⁴ indicate that the solubilities of these phases do not differ

105 significantly in the absence of alkali. The availability of a comprehensive set of solubility

^b This notation includes products with and without Al (*i.e.* C-(N,K-)S-H), although effort is made to distinguish these phases in the text.

106 data for C-(N,K-)A-S-H is necessary for the development of more accurate thermodynamic
107 models for this phase,²⁸ which would advance the utility of thermodynamic modelling in the
108 description and performance prediction of cement-based materials. Therefore, this paper aims
109 to clarify the effects of Na, K, Al and Ca on the chemical composition, structure, and
110 solubility of C-(N,K-)A-S-H, utilising a dataset for C-(N,K-)A-S-H equilibrated at 50°C. The
111 results presented are particularly relevant for cements used for construction in large structures
112 which experience a significant semi-adiabatic temperature rise during hydration (e.g. dams or
113 foundations), or in warm climates. The results are also discussed with respect to existing
114 solubility data at ambient conditions.

115

116 **2. Materials and methods**

117

118 **2.1 C-(N,K-)A-S-H synthesis**

119

120 C-(N,K-)A-S-H samples were synthesised at bulk molar Al/Si ratios (Al/Si*) of 0 to 0.1 and
121 bulk molar Ca/Si ratios (Ca/Si*) of 0.6 to 1.6 using Milli-Q water (Merck Millipore) and 0 to
122 1 M solutions of NaOH and/or KOH (Merck Millipore), at a solution/solid ratio of 45 in a N₂-
123 filled glovebox by the method described in ^{8, 14}. Samples were equilibrated at 50°C in
124 polyethylene vessels and shaken twice per week, then filtered in a N₂-filled glovebox 56 days
125 after synthesis, and freeze-dried for a week. Freeze-dried solids were stored in N₂-filled
126 desiccators at ~30% relative humidity (over saturated CaCl₂ solutions) until analysis.

127

128 **2.2 Experimental characterisation techniques**

129

130 A Dionex DP ICS-3000 ion chromatograph was used to determine Ca, Si, Al, Na and K
131 concentrations in the filtrates (relative measurement error ±10% in the concentration range of

132 interest). Aqueous hydroxide concentrations were determined at $\sim 24^\circ\text{C}$ with a Knick pH
133 meter (pH-Meter 766) and a Knick SE100 electrode, which was calibrated against KOH or
134 NaOH solutions of known concentrations. Thermogravimetric analysis (TGA) was performed
135 using a Mettler Toledo TGA/SDTA851^e at a heating rate of $20^\circ\text{C}/\text{min}$ under an N_2
136 atmosphere, and derivative thermograms were calculated numerically. Powder XRD patterns
137 were recorded on a PANalytical X'Pert Pro MDF diffractometer using a Ge(111) Johansson
138 monochromator for Cu $K\alpha$ radiation, an X'Celerator detector, and a step size of $0.017^\circ 2\theta$. An
139 external CaF_2 standard was used for Rietveld analysis to quantify of the amount of crystalline
140 phases in each sample.³⁶ The ion chromatography (IC) and pH measurements, initial
141 synthesis conditions, and solid phase assemblages and water content as determined by TGA,
142 XRD and Rietveld analysis, were used in mass balance calculations to determine chemical
143 compositions of the C-(N,K-)A-S-H products formed.

144

145 Solid-state ^{29}Si magic angle spinning nuclear magnetic resonance (MAS NMR) spectra were
146 collected for the Al-free and $\text{Al}/\text{Si}^* = 0.1$ samples synthesised with water, with 0.5 M NaOH,
147 and with 0.5 M NaOH and 0.5 M KOH (denoted 0.5 M NaOH/0.5 M KOH) at 79.49 MHz on
148 a Bruker Avance 400 MHz NMR spectrometer with a 7 mm CP/MAS probe. The
149 measurements were recorded using a 4500 Hz spinning rate, 9216 scans, $\pi/3$ pulses of 2.5 μs ,
150 and a 20 s relaxation delay. ^{29}Si chemical shifts were referenced to external tetramethylsilane.
151 Spectral deconvolutions were carried out using component peaks with a Lorentzian/Gaussian
152 ratio of 0.5, full width at half height ≤ 3 ppm, and peak amplitudes constrained to be
153 consistent with the tobermorite-like structures present in C-(N,K-)A-S-H (Appendix S1,
154 Electronic Supporting Information).³⁷ The percentages of Al in the cross-linked components
155 ($Al_{[C]}$) of the C-(N,K-)A-S-H products formed here are calculated using the 'Cross-linked
156 Substituted Tobermorite Model' (CSTM) (eq.(1)):³⁷

157

$$Al_{[C]} = 100 \frac{(Al/Si)_{[C]} [Q^1 + Q^2(1Al) + Q^2 + Q^3(1Al) + Q^3]_{[C]}}{\sum_k ((Al/Si)_k [Q^1 + Q^2(1Al) + Q^2 + Q^3(1Al) + Q^3]_k)} \quad (1)$$

159

160 where the cross-linked and non-cross-linked components of C-(N,K-)A-S-H are represented
 161 by subscripts [C] and [NC] respectively, $k \in \{[C], [NC]\}$ and the Al/Si fractions in this
 162 formula are calculated according to eqs.(2,3):

163

$$(Al/Si)_{[C]} = \frac{Q^3(1Al)}{Q^1 + Q^2 + Q^2(1Al) + Q^3 + Q^3(1Al)} \quad (2)$$

165

$$(Al/Si)_{[NC]} = \frac{(\frac{1}{2})Q^2(1Al)}{Q^1 + Q^2 + Q^2(1Al)} \quad (3)$$

167

168 These parameters are used directly in eq.(4) to calculate overall Al/Si ratios of the C-(N,K-
 169)A-S-H products formed here; this correctly describes the composition of mixed cross-
 170 linked/non-cross-linked C-(N,K-)A-S-H according to the CSTM formulation:³⁷

171

$$(Al/Si)_{C-(N,K-)A-S-H} = \frac{\left[\frac{(Al/Si)_{[NC]}}{(1+(Al/Si)_{[NC]})} \right] (Al+Si)_{[NC]} + \left[\frac{(Al/Si)_{[C]}}{(1+(Al/Si)_{[C]})} \right] (Al+Si)_{[C]}}{\left[\frac{1}{(1+(Al/Si)_{[NC]})} \right] (Al+Si)_{[NC]} + \left[\frac{1}{(1+(Al/Si)_{[C]})} \right] (Al+Si)_{[C]}} \quad (4)$$

173

174 where $(Al+Si)$ indicates the total amount of Al and Si in a C-(N,K-)A-S-H component ([C]
 175 or [NC]).

176

177 **2.3 Thermodynamic modelling**

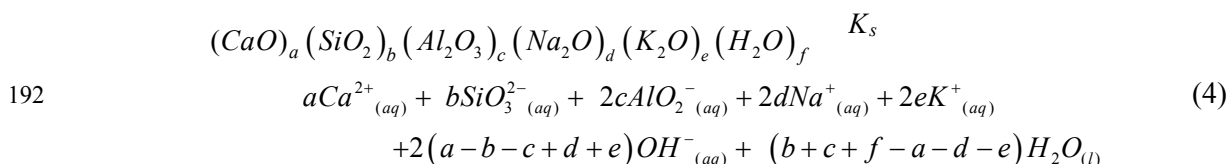
178

179 Thermodynamic modelling was performed in the GEM Selektor v.3 software
 180 (<http://gems.web.psi.ch/>)^{38, 39} using the PSI/Nagra 12/07 thermodynamic database,⁴⁰ which is
 181 updated from⁴¹ via the inclusion of two additional aqueous (alumino)silicate species, and the
 182 CEMDATA07 thermodynamic database⁴²⁻⁴⁹ updated to include recently published data for
 183 Al(OH)₃, hydrogarnet and C-(N,K-)A-S-H.^{28, 50, 51} Activity coefficients were calculated using
 184 the extended Debye-Hückel equation (in Truesdell-Jones form) with the ion size and
 185 extended term parameter for KOH ($\hat{a} = 3.67 \text{ \AA}$ and $b_{\gamma} = 0.123 \text{ kg/mol}$).⁵² The thermodynamic
 186 properties of the aqueous species and solid phases used in these calculations are shown in
 187 Appendix S2 (Electronic Supporting Information).

188

189 Solubility products (K_s) for C-(N,K-)A-S-H were calculated from the generalised dissolution
 190 reaction shown in eq.(5):

191



193

194 where a , b , c , d , e and f are the respective stoichiometric coefficients for CaO, SiO₂, Al₂O₃,
 195 Na₂O, K₂O and H₂O in C-(N,K-)A-S-H. This reaction implies the following relationship for
 196 K_s (eq.(6)):

197

$$\begin{aligned}
 K_s = & \left\{ Ca^{2+}_{(aq)} \right\}^a \cdot \left\{ SiO_3^{2-}_{(aq)} \right\}^b \cdot \left\{ AlO_2^{-}_{(aq)} \right\}^{2c} \\
 & \cdot \left\{ Na^{+}_{(aq)} \right\}^{2d} \cdot \left\{ K^{+}_{(aq)} \right\}^{2e} \cdot \left\{ OH^{-}_{(aq)} \right\}^{2(a-b-c+d+e)} \cdot \left\{ H_2O_{(l)} \right\}^{(b+c+f-a-d-e)} \quad (4)
 \end{aligned}$$

198

199

200 Activities of $\text{Ca}^{2+}_{(\text{aq})}$, $\text{SiO}_3^{2-}_{(\text{aq})}$, $\text{AlO}_2^{-}_{(\text{aq})}$, $\text{Na}^{+}_{(\text{aq})}$, $\text{K}^{+}_{(\text{aq})}$, $\text{OH}^{-}_{(\text{aq})}$ and $\text{H}_2\text{O}_{(\text{l})}$ species were
201 calculated with GEM-Selektor v.3,^{38, 39} using the measured concentrations of Ca, Si, Al, Na,
202 K and OH⁻ in the supernatants.

203

204 3. Results and discussion

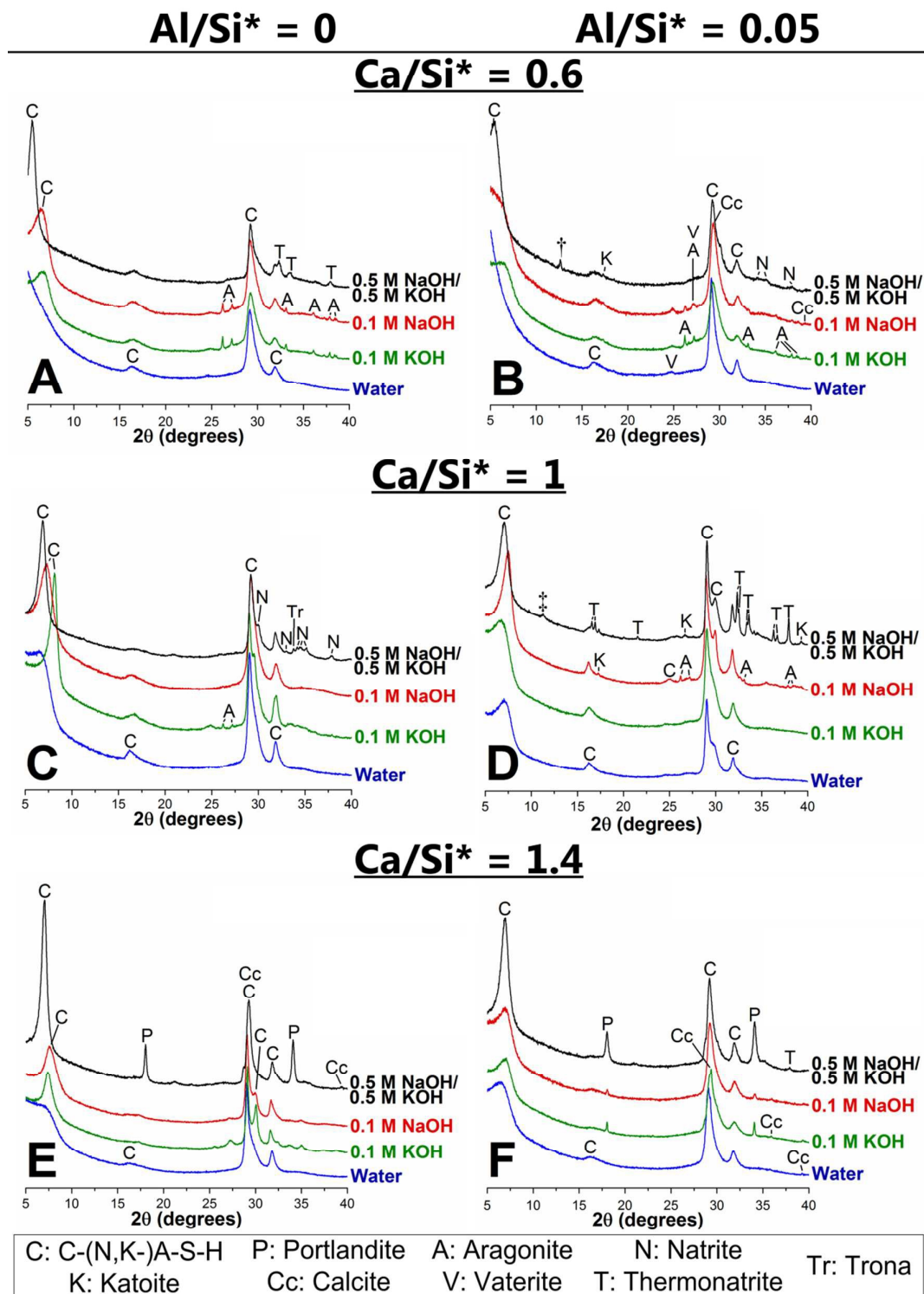
205

206 3.1 Solid phase analysis

207

208 The XRD results (Figure 2) show that the main solid phase formed in each of the Al-free
209 samples is C-(N,K-)S-H (phase quantification is presented as Electronic Supporting
210 Information, Appendix S3). This is the only reaction product identified in the samples
211 synthesised with Ca/Si* ratios of 0.6 and 1 by XRD and TGA (Electronic Supporting
212 Information, Appendix S4). Reflections assigned to portlandite ($\text{Ca}(\text{OH})_2$, Powder Diffraction
213 File (PDF)# 00-044-1481) are only present in the data for the Al-free sample synthesised with
214 0.5 M NaOH/0.5 M KOH at a Ca/Si* ratio of 1.4, although portlandite is also identified in
215 some other Al-free samples synthesised with alkali hydroxide solutions and Ca/Si* ratios \geq
216 1.2. Portlandite has been observed in C-(N,K-)S-H samples cured for 3 weeks or longer at
217 25°C with Ca/Si* ratios > 1 and $[\text{NaOH}] \geq 1 \text{ M}$,^{9, 23} in good agreement with these results.
218 Calcite (CaCO_3 , PDF# 00-005-0586), aragonite (CaCO_3 , PDF# 00-041-1475), natrite
219 (Na_2CO_3 , PDF# 01-075-6816), thermonatrite ($\text{Na}_2\text{CO}_3 \cdot \text{H}_2\text{O}$, PDF# 00-005-0586) and trona
220 ($\text{Na}_3\text{H}(\text{CO}_3)_2 \cdot 2\text{H}_2\text{O}$, PDF# 01-078-1064) are present in some of the samples, formed by
221 superficial carbonation during preparation and/or analysis.

222



223
224
225
226
227
228

Figure 2. Cu K α diffractograms of C-(N,K-)A-S-H samples equilibrated at 50°C: A) Ca/Si* = 0.6 and Al/Si* = 0; B) Ca/Si* = 0.6 and Al/Si* = 0.05; C) Ca/Si* = 1 and Al/Si* = 0; D) Ca/Si* = 1 and Al/Si* = 0.05; E) Ca/Si* = 1.4 and Al/Si* = 0; and F) Ca/Si* = 1.4 and Al/Si* = 0.05. The peaks marked by † and ‡ are tentatively assigned to K-natrolite and carbonated calcium hemicarboaluminate hydrate. Ca/Si* = bulk Ca/Si. Al/Si* = bulk Al/Si.

229 The solid reaction products identified in the C-(N,K-)A-S-H samples with Al/Si* = 0.05 are
230 similar to those identified in their Al-free counterparts: the main reaction product in each
231 specimen is C-(N,K-)A-S-H, and portlandite is only identified in samples synthesised with
232 0.1 M and 1 M alkali hydroxide solutions at Ca/Si* ratios ≥ 1.2 (Figure 2). Katoite
233 ((CaO)₃(Al₂O₃)(H₂O)₆, PDF# 00-024-0217) is additionally present in some samples, although
234 only in minor amounts (≤ 2 wt.% of the total sample mass). The superficial carbonation
235 products calcite, aragonite, vaterite (CaCO₃, PDF# 04-015-9018), natrite and thermonatrite
236 are identified in some of the Al-containing samples. These phase assemblages are similar to
237 those identified by XRD in C-(N,K-)A-S-H samples synthesised using the same method and
238 bulk chemical compositions but at 20°C.⁸ The small peaks at 12.6° 2 θ and 11.3° 2 θ in the
239 diffractograms of the Ca/Si* = 0.6 and Ca/Si* = 1 samples synthesised with 0.5 M NaOH/0.5
240 M KOH are tentatively assigned to K-natrolite (PDF# 01-080-0519)⁵³ and carbonated
241 calcium hemicarboaluminate hydrate ($0.125 < C/Ca < 0.25$),⁵⁴ respectively.

242

243 The C-(N,K-)A-S-H products in the alkali-containing samples are much more crystalline than
244 the specimen prepared in the absence of alkalis, as identified by the much clearer and sharper
245 (002) reflections between 5 and 10° 2 θ in the presence of Na and/or K (Figure 2). The effects
246 of C-(N,K-)A-S-H chemical composition and alkali hydroxide concentration on the (002)
247 reflections are presented in section 3.3 below.

248

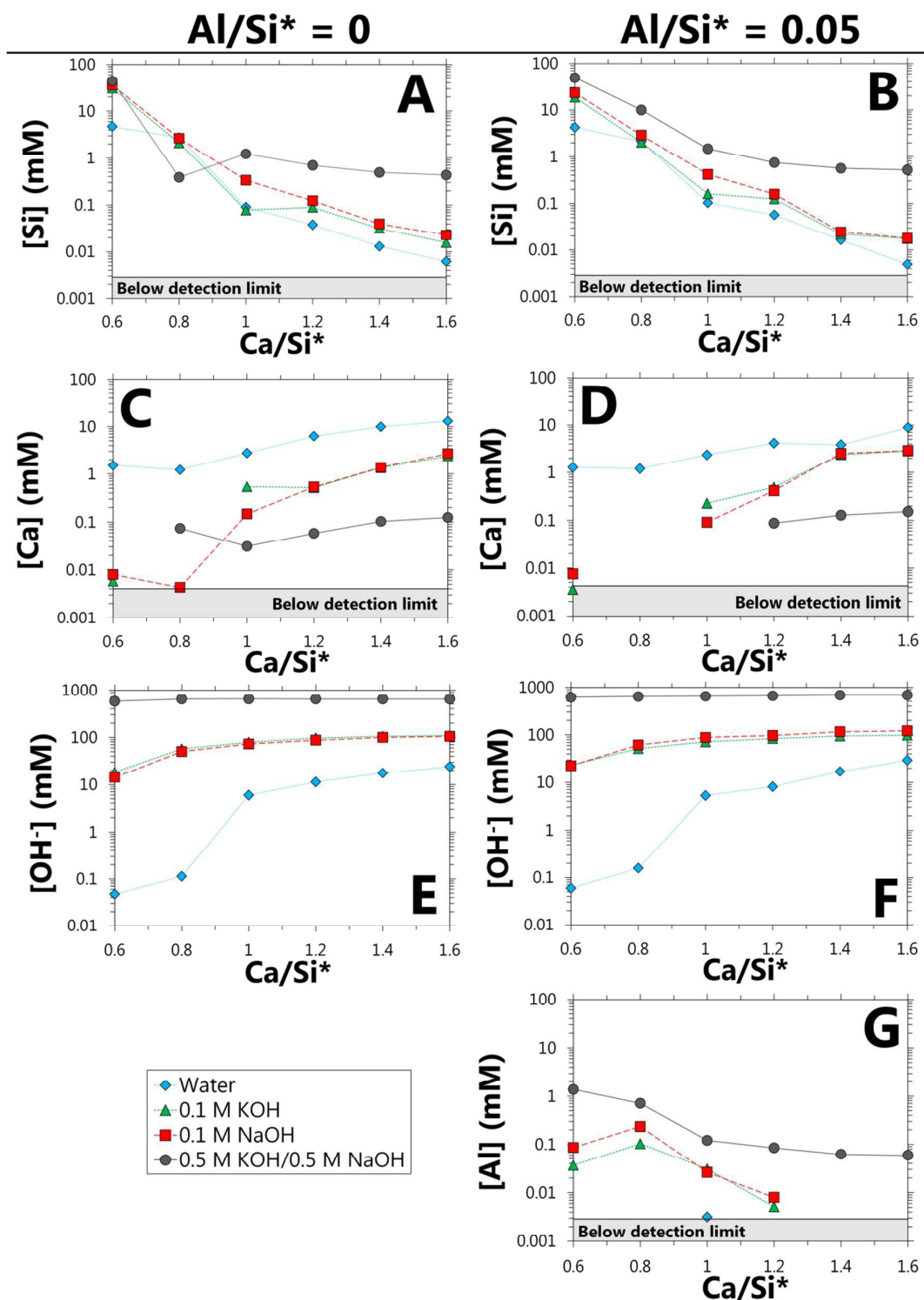
249 3.2 Aqueous phase analysis

250

251 The measured concentrations of Si, Ca and OH⁻ in the supernatants of the C-(N,K-)A-S-H
252 samples do not change greatly as a function of the bulk Al concentration (Figure 3). In
253 general, the measured aqueous Si and OH⁻ concentrations are higher and the dissolved Ca

254 concentrations are lower in samples synthesised with solutions containing more alkalis. The
255 aqueous Si concentrations typically decrease and the dissolved Ca concentrations generally
256 increase as functions of the Ca/Si* ratio. The OH⁻ concentrations are generally greater and
257 less dependent on chemical composition at higher bulk Ca content. These results are
258 consistent with existing solubility measurements in the CaO-(Na₂O,K₂O)-Al₂O₃-SiO₂-H₂O
259 systems at ~25°C,^{21-24, 35, 55, 56} which show the same trends in dissolved Si, Ca and OH⁻
260 concentrations with respect to the bulk alkali content and Ca/Si ratio. Here, dissolved Al
261 concentrations were generally found to be lower at higher Ca/Si* ratios, and higher in
262 samples more highly concentrated in alkalis.

263



264
265
266
267
268
269
270
271

Figure 3. Concentrations of dissolved Si, Ca, OH^- and Al in the supernatants of the C-(N,K-)A-S-H samples: A) $[\text{Si}]$, $\text{Al/Si}^* = 0$; B) $[\text{Si}]$, $\text{Al/Si}^* = 0.05$; C) $[\text{Ca}]$, $\text{Al/Si}^* = 0$; D) $[\text{Ca}]$, $\text{Al/Si}^* = 0.05$; E) $[\text{OH}^-]$, $\text{Al/Si}^* = 0$; F) $[\text{OH}^-]$, $\text{Al/Si}^* = 0.05$; G) $[\text{Al}]$, $\text{Al/Si}^* = 0.05$. OH^- concentrations are calculated from pH measurements at $\sim 24^\circ\text{C}$. The estimated relative uncertainty of the IC measurements is $\pm 10\%$. $\text{Ca/Si}^* = \text{bulk Ca/Si}$. $\text{Al/Si}^* = \text{bulk Al/Si}$. Lines are for eye-guides only. These results are tabulated in Appendix S6 (Electronic Supporting Information).

272 Dissolved Si, Ca and OH⁻ concentrations in the sample sets synthesised with 0.1 M KOH and
273 with 0.1 M NaOH are equal for Ca/Si* \geq 1.2, and are also similar for most samples with
274 lower Ca content (Figure 3). This result suggests that C-(N,K-)A-S-H solubility does not vary
275 greatly as a function of the nature of the alkali cation (Na or K) present. However, the large
276 changes in dissolved Si, Ca, OH⁻ and Al concentrations as functions of the bulk alkali
277 concentration and the Ca/Si ratio indicate that C-(N,K-)A-S-H solubility may change
278 significantly with respect to these parameters, as will be discussed further in section 3.4.
279 Saturation indices calculated using the measured aqueous Si, Ca, OH⁻ and Al concentrations
280 shown in Figure 3 indicate that the samples containing katoite (*e.g.* the Ca/Si* = 1, Al/Si* =
281 0.05, 0.5 M NaOH/0.5 M KOH sample, see Figure 2) did not reach equilibrium within the
282 experimental timeframe here, as this phase is calculated to be undersaturated in the systems
283 analysed. There was otherwise good agreement between the phase assemblages formed and
284 the calculated saturation indices. These results are presented in detail as Electronic
285 Supporting Information (Appendix S5).

286

287 **3.3 C-(N,K-)A-S-H chemical composition and basal spacing**

288

289 Chemical compositions of the C-(N,K-)A-S-H products formed at Al/Si* ratios = 0 and 0.05
290 are shown in Tables 1 and 2. Most of the C-(N,K-)A-S-H products formed at $0.6 \leq$ Ca/Si*
291 ratios \leq 1.4 have Ca/Si and Al/Si ratios similar to the bulk synthesis conditions used in the
292 samples synthesised with water and 0.1 M alkali solutions, due to the relatively low levels of
293 secondary or superficial carbonation products formed in these specimen (yield is \geq 91 wt.%
294 C-(N,K-)A-S-H in these samples; Appendix S3, Electronic Supporting Information). Samples
295 synthesised with Ca/Si* ratios = 1.6 and alkali hydroxide solutions contain more portlandite
296 due to the decreased solubility of this phase at higher Ca and alkali content (Tables 1 and 2).

297 Table 1. Chemical compositions of the C-(N,K-)S-H products ($Al/Si^* = 0$), determined from Rietveld analysis and IC, TGA, XRD and pH
 298 measurements (normal font), and from IC, TGA and pH measurements considering C-(N,K-)S-H and portlandite only (italic font). The estimated
 299 absolute errors are ± 0.05 units in the $Ca/(Al+Si)$ ratios, ± 0.2 units in the $H_2O/(Al+Si)$ ratios, and ± 0.08 units for the 0.1 M alkali samples and
 300 ± 0.7 for the 1 M alkali samples in the $(Na+K)/(Al+Si)$ ratios of the C-(N,K-)S-H products. $Ca/Si^* = \text{bulk } Ca/Si$.

Synthesis solution	C-(N,K-)S-H chemical formula	Ca/Si	Na/Si	K/Si	H ₂ O/Si
Ca/Si* = 0.6					
Water	$(CaO)_{0.61}(SiO_2)_1(H_2O)_{1.1}$	0.61	n/a ^a	n/a ^b	1.1
0.1 M NaOH	$(CaO)_{0.70}(Na_2O)_{0.11}(SiO_2)_1(H_2O)_{1.6}$	0.70	0.23	n/a ^b	1.6
0.1 M KOH	$(CaO)_{0.69}(K_2O)_{0.13}(SiO_2)_1(H_2O)_{1.6}$	0.69	n/a ^a	0.27	1.6
0.5 M NaOH/0.5 M KOH	$(CaO)_{0.73}(Na_2O)_{0.04}(K_2O)_{0.08}(SiO_2)_1(H_2O)_{1.7}$	0.73	0.08	0.16	1.7
Ca/Si* = 0.8					
Water	$(CaO)_{0.80}(SiO_2)_1(H_2O)_{1.9}$	0.80	n/a ^a	n/a ^b	1.9
0.1 M NaOH	$(CaO)_{0.81}(Na_2O)_{0.09}(SiO_2)_1(H_2O)_{1.5}$	0.81	0.18	n/a ^b	1.5
0.1 M KOH	$(CaO)_{0.81}(K_2O)_{0.10}(SiO_2)_1(H_2O)_{1.3}$	0.81	n/a ^a	0.21	1.3
0.5 M NaOH/0.5 M KOH	$(CaO)_{0.3}(Na_2O)_{0.02}(K_2O)_{0.02}(SiO_2)_1(H_2O)_{1.1}$ ^c	0.30 ^c	0.03 ^c	0.04 ^c	1.1 ^c
Ca/Si* = 1					
Water	$(CaO)_{1.0}(SiO_2)_1(H_2O)_{1.4}$	1.0	n/a ^a	n/a ^b	1.4
0.1 M NaOH	$(CaO)_{1.0}(Na_2O)_{0.06}(SiO_2)_1(H_2O)_{1.3}$	1.0	0.12	n/a ^b	1.3
0.1 M KOH	$(CaO)_{1.0}(K_2O)_{0.07}(SiO_2)_1(H_2O)_{1.6}$	1.0	n/a ^a	0.13	1.6
0.5 M NaOH/0.5 M KOH	$(CaO)_{1.0}(Na_2O)_{0.07}(K_2O)_{0.08}(SiO_2)_1(H_2O)_{1.7}$	1.0	0.15	0.17	1.7
Ca/Si* = 1.2					
Water	$(CaO)_{1.2}(SiO_2)_1(H_2O)_{1.5}$	1.2	n/a ^a	n/a ^b	1.5
0.1 M NaOH	$(CaO)_{1.2}(Na_2O)_{0.02}(SiO_2)_1(H_2O)_{1.4}$	1.2	0.05	n/a ^b	1.4
0.1 M KOH	$(CaO)_{1.2}(K_2O)_{0.03}(SiO_2)_1(H_2O)_{1.6}$	1.2	n/a ^a	0.06	1.6
0.5 M NaOH/0.5 M KOH	$(CaO)_{1.0}(Na_2O)_{0.09}(K_2O)_{0.08}(SiO_2)_1(H_2O)_{2.0}$	1.0	0.19	0.16	2.0
Ca/Si* = 1.4					
Water	$(CaO)_{1.3}(SiO_2)_1(H_2O)_{1.9}$	1.3	n/a ^a	n/a ^b	1.9
0.1 M NaOH	$(CaO)_{1.4}(SiO_2)_1(H_2O)_{1.7}$	1.4	<0.01	n/a ^b	1.7
0.1 M KOH	$(CaO)_{1.4}(K_2O)_{0.02}(SiO_2)_1(H_2O)_{1.9}$	1.4	n/a ^a	0.03	1.9
0.5 M NaOH/0.5 M KOH	$(CaO)_{1.4}(Na_2O)_{0.09}(K_2O)_{0.08}(SiO_2)_1(H_2O)_{2.1}$	1.4	0.18	0.16	2.1

301

302

Table 1. Continued.

Ca/Si* = 1.6					
Water	$(CaO)_{1.5}(SiO_2)_1(H_2O)_{2.0}$	1.5	<i>n/a</i> ^a	<i>n/a</i> ^b	2.0
0.1 M NaOH	$(CaO)_{1.4}(SiO_2)_1(H_2O)_{1.8}$	1.4	<0.01	<i>n/a</i> ^b	1.8
0.1 M KOH	$(CaO)_{1.4}(K_2O)_{0.01}(SiO_2)_1(H_2O)_{1.7}$	1.4	<i>n/a</i> ^a	0.02	1.7
0.5 M NaOH/0.5 M KOH	$(CaO)_{1.3}(SiO_2)_1(H_2O)_{1.1}$	1.3	<0.01	<0.01	1.1

303 ^a n/a = not applicable: no Na was added during synthesis (<0.6 mM Na is present as an impurity in the 0.1 M KOH synthesis solution).

304 ^b n/a = not applicable: no K was added during synthesis.

305 ^c An additional major phase, possibly a zeolite, was formed in this sample in addition to C-(N,K-)S-H.

306 Table 2. Chemical compositions of the C-(N,K-)A-S-H products ($Al/Si^* = 0.05$), determined from Rietveld analysis and IC, TGA, XRD and pH
 307 measurements (normal font), and from IC, TGA and pH measurements considering C-(N,K-)S-H and portlandite only (italic font). The estimated
 308 absolute errors are ± 0.05 units in the $Ca/(Al+Si)$ ratios, ± 0.2 units in the $H_2O/(Al+Si)$ ratios, ± 0.02 units in the Al/Si ratios, and ± 0.08 units for
 309 the 0.1 M alkali samples and ± 0.7 for the 1 M alkali samples in the $(Na+K)/(Al+Si)$ ratios of the C-(N,K-)A-S-H products. $Ca/Si^* = \text{bulk } Ca/Si$.

Synthesis solution	C-(N,K-)A-S-H chemical formula	Ca/(Al+Si)	Al/Si	Na/(Al+Si)	K/(Al+Si)	H ₂ O/(Al+Si)
Ca/Si* = 0.6						
Water	$(CaO)_{0.60}(Al_2O_3)_{0.026}(SiO_2)_1(H_2O)_{1.4}$	0.57	0.051	n/a ^a	n/a ^b	1.3
0.1 M NaOH	$(CaO)_{0.66}(Al_2O_3)_{0.28}(Na_2O)_{0.13}(SiO_2)_1(H_2O)_{1.7}$	0.63	0.055	0.25	n/a ^b	1.6
0.1 M KOH	$(CaO)_{0.65}(Al_2O_3)_{0.027}(K_2O)_{0.13}(SiO_2)_1(H_2O)_{1.2}$	0.62	0.054	n/a ^a	0.24	1.1
0.5 M NaOH/0.5 M KOH	$(CaO)_{0.76}(Al_2O_3)_{0.028}(Na_2O)_{0.13}(K_2O)_{0.13}(SiO_2)_1(H_2O)_{1.9}$	0.72	0.056	0.24	0.24	1.8
Ca/Si* = 0.8						
Water	$(CaO)_{0.80}(Al_2O_3)_{0.025}(SiO_2)_1(H_2O)_{1.7}$	0.76	0.051	n/a ^a	n/a ^b	1.6
0.1 M NaOH	$(CaO)_{0.81}(Al_2O_3)_{0.25}(Na_2O)_{0.11}(SiO_2)_1(H_2O)_{1.4}$	0.77	0.050	0.21	n/a ^b	1.3
0.1 M KOH	$(CaO)_{0.81}(Al_2O_3)_{0.025}(K_2O)_{0.10}(SiO_2)_1(H_2O)_{1.2}$	0.77	0.050	n/a ^a	0.19	1.1
0.5 M NaOH/0.5 M KOH	$(CaO)_{0.84}(Al_2O_3)_{0.024}(Na_2O)_{0.18}(K_2O)_{0.17}(SiO_2)_1(H_2O)_{2.8}$	0.80	0.049	0.35	0.33	2.7
Ca/Si* = 1						
Water	$(CaO)_{0.99}(Al_2O_3)_{0.025}(SiO_2)_1(H_2O)_{1.5}$	0.94	0.050	n/a ^a	n/a ^b	1.4
0.1 M NaOH	$(CaO)_{1.0}(Al_2O_3)_{0.023}(Na_2O)_{0.06}(SiO_2)_1(H_2O)_{1.3}$	1.00	0.045	0.12	n/a ^b	1.3
0.1 M KOH	$(CaO)_{1.0}(Al_2O_3)_{0.025}(K_2O)_{0.06}(SiO_2)_1(H_2O)_{1.3}$	0.95	0.050	n/a ^a	0.11	1.3
0.5 M NaOH/0.5 M KOH	$(CaO)_{1.0}(Al_2O_3)_{0.025}(Na_2O)_{0.13}(K_2O)_{0.10}(SiO_2)_1(H_2O)_{1.8}$	0.96	0.050	0.25	0.20	1.7
Ca/Si* = 1.2						
Water	$(CaO)_{1.2}(Al_2O_3)_{0.025}(SiO_2)_1(H_2O)_{1.8}$	1.12	0.050	n/a ^a	n/a ^b	1.7
0.1 M NaOH	$(CaO)_{1.2}(Al_2O_3)_{0.025}(Na_2O)_{0.04}(SiO_2)_1(H_2O)_{1.5}$	1.14	0.050	0.08	n/a ^b	1.4
0.1 M KOH	$(CaO)_{1.2}(Al_2O_3)_{0.025}(K_2O)_{0.02}(SiO_2)_1(H_2O)_{1.4}$	1.14	0.050	n/a ^a	0.04	1.4
0.5 M NaOH/0.5 M KOH	$(CaO)_{1.0}(Al_2O_3)_{0.025}(Na_2O)_{0.14}(K_2O)_{0.10}(SiO_2)_1(H_2O)_{1.8}$	0.99	0.050	0.26	0.20	1.7
Ca/Si* = 1.4						
Water	$(CaO)_{1.4}(Al_2O_3)_{0.025}(SiO_2)_1(H_2O)_{1.9}$	1.3	0.050	n/a ^a	n/a ^b	1.8
0.1 M NaOH	$(CaO)_{1.4}(Al_2O_3)_{0.025}(Na_2O)_{0.02}(SiO_2)_1(H_2O)_{1.8}$	1.3	0.050	0.05	n/a ^b	1.8
0.1 M KOH	$(CaO)_{1.4}(Al_2O_3)_{0.025}(SiO_2)_1(H_2O)_{1.5}$	1.3	0.050	n/a ^a	<0.01	1.4
0.5 M NaOH/0.5 M KOH	$(CaO)_{1.2}(Al_2O_3)_{0.025}(Na_2O)_{0.12}(K_2O)_{0.10}(SiO_2)_1(H_2O)_{1.7}$	1.2	0.050	0.23	0.19	1.6

310

311

Table 2. Continued.

Ca/Si* = 1.6						
Water	$(CaO)_{1.5}(Al_2O_3)_{0.025}(SiO_2)_1(H_2O)_{2.1}$	1.5	0.050	<i>n/a</i> ^a	<i>n/a</i> ^b	2.0
0.1 M NaOH	$(CaO)_{1.3}(Al_2O_3)_{0.025}(Na_2O)_{0.02}(SiO_2)_1(H_2O)_{1.7}$	1.3	0.050	0.03	<i>n/a</i> ^b	1.7
0.1 M KOH	$(CaO)_{1.3}(Al_2O_3)_{0.025}(SiO_2)_1(H_2O)_{1.5}$	1.2	0.050	<i>n/a</i> ^a	<0.01	1.4
0.5 M NaOH/0.5 M KOH	$(CaO)_{1.2}(Al_2O_3)_{0.025}(Na_2O)_{0.15}(K_2O)_{0.12}(SiO_2)_1(H_2O)_{1.8}$	1.2	0.050	0.29	0.23	1.7

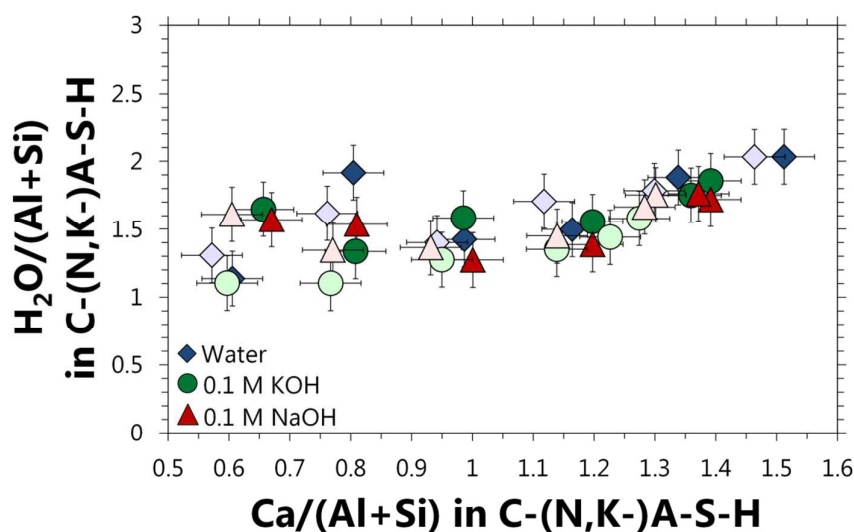
312 ^a n/a = not applicable: no Na was added during synthesis (<0.6 mM Na is present as an impurity in the 0.1 M KOH synthesis solution).

313 ^b n/a = not applicable: no K was added during synthesis.

314

315 The C-(N,K-)A-S-H products typically contain $H_2O/(Al+Si)$ ratios between 1 and 2 (Figure
 316 4): the H_2O content in C-(N,K-)A-S-H was determined by assigning the mass losses between
 317 30°C and 550°C to the decomposition of C-(N,K-)A-S-H, portlandite, katoite and $Al(OH)_3$
 318 during heating by TGA (Appendix S4, Electronic Supporting Information). Portlandite was
 319 the only secondary product quantified by TGA and used in C-(N,K-)A-S-H chemical
 320 composition calculations in the absence of XRD data; the formation of only very small
 321 quantities of other secondary products here (≤ 2 wt.% of the total mass of each sample)
 322 means that any errors introduced into the reported C-(N,K-)A-S-H chemical compositions
 323 due to use of this method are minor.

324



325

326

327

328

329

330

331

Figure 4. $H_2O/(Al+Si)$ ratios of the ($Al/Si^* = 0$) C-(N,K-)S-H (dark symbols) and $Al/Si^* = 0.05$ C-(N,K-)A-S-H (light symbols) as functions of the $Ca/(Al+Si)$ ratio, for samples synthesised with ≤ 0.1 M alkali hydroxide solutions and equilibrated at 50°C. The estimated absolute errors are ± 0.05 units in the $Ca/(Al+Si)$ ratios and ± 0.2 in the $H_2O/(Al+Si)$ ratios of the C-(N,K-)A-S-H products.

332 The reported $H_2O/(Al+Si)$ ratios (Figure 4) are in relatively good agreement with the
 333 expected result for C-(N,K-)A-S-H equilibrated at $\sim 30\%$ RH, where no ‘free’ water is present
 334 and some adsorbed water is removed,^{57, 58} and with the H_2O content of C-(N,K-)A-S-H
 335 synthesised at 20°C.⁸ In general, the $H_2O/(Al+Si)$ ratios increase slightly as a direct function

336 of the $\text{Ca}/(\text{Al}+\text{Si})$ ratios of the C-(N,K-)A-S-H products formed, but no significant
337 correlations are found between the $\text{H}_2\text{O}/(\text{Al}+\text{Si})$ ratio and the alkali or Al content in this
338 phase. A strong direct relationship between the $\text{H}_2\text{O}/(\text{Al}+\text{Si})$ and $\text{Ca}/(\text{Al}+\text{Si})$ ratios is reported
339 for laboratory-synthesised C-S-H,⁵⁹ but is not as evident here from the data in presented in
340 Figure 4. Chemical compositions of the C-(N,K-)A-S-H products synthesised using 0.5 M
341 NaOH/0.5 KOH solutions are omitted from Figure 4 due to the relatively higher quantities of
342 secondary products formed in these samples.

343

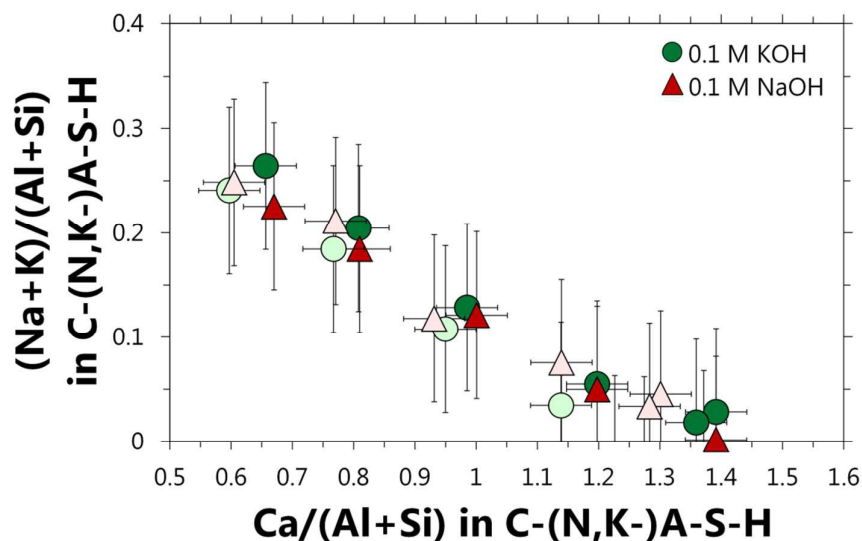
344 The alkali and Al contents of the C-(N,K-)A-S-H products formed are independent of each
345 other when relatively low amounts of Al are present (comparing the darker-coloured symbols
346 with $\text{Al}/\text{Si}^* = 0$ to the lighter-coloured symbols with $\text{Al}/\text{Si}^* = 0.05$ in Figure 5). At Al/Si^*
347 ratios ≤ 0.05 , all of the Al added is generally incorporated into C-(N,K-)A-S-H products
348 when synthesised with water and no added alkalis (Table 2).¹⁴ However, the amount of Al
349 which can be incorporated into C-(N,K-)A-S-H is related to the dissolved concentration of
350 this element at higher bulk Al content: increasing the bulk Na or K concentration increases
351 the amount of dissolved Al (Figure 3) and consequently also the amount of Al which can be
352 incorporated into C-(N,K-)A-S-H.⁸ This description is consistent with ²⁹Si MAS NMR
353 analysis of hydrated white Portland cement with different alkali contents,³³ which showed the
354 formation of C-(N,K-)A-S-H products with increased Al/Si ratios at higher bulk alkali
355 concentration. This description is also in agreement with the lack of a direct relationship
356 found in ¹¹ between alkali and Al content in laboratory-synthesised C-(N,K-)S-H, and in C-
357 (N,K-)A-S-H with $\text{Al}/\text{Si} = 0.04$ in hydrated blends of PC and silica fume.

358

359 The amount of Na and K incorporated in the C-(N,K-)A-S-H products decreases with the
360 $\text{Ca}/(\text{Al}+\text{Si})$ ratio of this phase (Figure 5), from $(\text{Na}+\text{K})/(\text{Al}+\text{Si}) = 0.25$ at $\text{Ca}/(\text{Al}+\text{Si}) = 0.6$ to

361 zero Na and K incorporated at $\text{Ca}/(\text{Al}+\text{Si}) = 1.6$. This trend, and the quantified
 362 $(\text{Na}+\text{K})/(\text{Al}+\text{Si})$ ratios, are consistent with those reported in earlier studies of alkali uptake in
 363 laboratory-synthesised C-(N,K-)A-S-H at room temperature.^{21, 25, 34, 60} The $(\text{Na}+\text{K})/(\text{Al}+\text{Si})$
 364 ratios of the C-(N,K-)A-S-H products are independent of the nature of the alkali element (Na
 365 or K).

366



367

368 Figure 5. Alkali cation uptake in C-(N,K-)S-H ($\text{Al}/\text{Si}^* = 0$, dark symbols) and $\text{Al}/\text{Si}^* = 0.05$
 369 C-(N,K-)A-S-H (light symbols) as functions of the $\text{Ca}/(\text{Al}+\text{Si})$ ratio, for samples synthesised
 370 with 0.1 M alkali hydroxide solutions at 50°C. The estimated absolute errors are ± 0.05 units
 371 in the $\text{Ca}/(\text{Al}+\text{Si})$ ratios and ± 0.08 units in the $(\text{Na}+\text{K})/(\text{Al}+\text{Si})$ ratios of the C-(N,K-)A-S-H
 372 products.

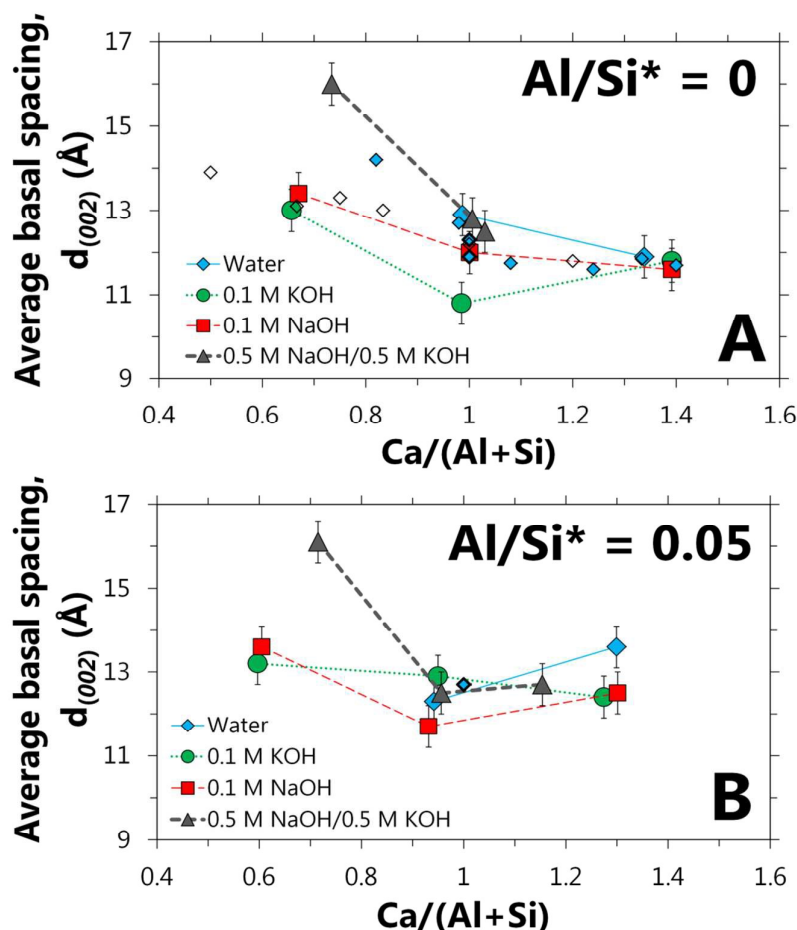
373

374 The increased alkali uptake determined here for C-(N,K-)A-S-H with lower $\text{Ca}/(\text{Al}+\text{Si})$ ratios
 375 (Figure 5) is explained here in terms of the incorporation of more alkali in C-(N,K-)A-S-H
 376 interlayer spaces at lower Ca content. This explanation is consistent with the largest basal
 377 spacings measured here at the lowest $\text{Ca}/(\text{Al}+\text{Si})$ ratios, at a fixed alkali hydroxide
 378 concentration (Figure 6). An inverse relationship between basal spacing and $\text{Ca}/(\text{Al}+\text{Si})$ ratio
 379 has also been reported for alkali-free calcium silicate hydrate⁶¹ and alkali-free calcium
 380 aluminosilicate hydrate (C-A-S-H) with $\text{Ca}/(\text{Al}+\text{Si})$ ratios < 1 .⁶²

381

382 The positions of the (002) reflections in Figure 6 correspond to average basal spacings of
 383 10.8-16 Å for the C-(N,K-)S-H products ($Al/Si^* = 0$) and average basal spacings of 11.7-16.1
 384 Å for the C-(N,K-)A-S-H products ($Al/Si^* = 0.05$). In addition to the incorporation of alkali
 385 in C-(N,K-)A-S-H interlayer spaces, this variation in basal spacing is also explained by the
 386 assignment of the C-(N,K-)A-S-H products formed to poorly-ordered structural analogues of
 387 orthorhombic 14 Å tobermorite (PDF# 00-029-0331), 11 Å tobermorite (PDF# 04-017-1028),
 388 9 Å tobermorite (PDF# 04-012-1761), a mixture of these minerals,⁶¹ or monoclinic
 389 clinotobermorite (PDF# 01-088-1328).⁵⁹

390



391

392

393 Figure 6. Average ($d_{(002)}$) basal spacings (estimated uncertainty = ± 0.5 Å) of the C-(N,K-)A-
 394 S-H products synthesised with A) $Al/Si^* = 0$ and B) $Al/Si^* = 0.05$ (large symbols). Small
 395 bold filled diamonds are data from samples equilibrated at 20°C in ⁸, small filled diamonds
 396 are data for 21-day old samples from ⁶², and small open diamonds are data from ⁶³. Al/Si^*
 397 represents the bulk Al/Si ratio.

398

399 For the C-(N,K-)S-H samples ($Al/Si^* = 0$), larger basal spacings are apparent in the water-
400 synthesised specimen than in some of the alkali-containing specimens (Figure 6A). Bach et
401 al.¹¹ reported the same trend for C-(N,K-)S-H synthesised at bulk $[NaOH] < 0.03$ M. Here,
402 the XRD results suggest that Na and K species are incorporated in C-(N,K-)S-H interlayers at
403 alkali concentrations ≥ 0.1 M, *i.e.* more aqueous Na and/or K species are incorporated into
404 interlayer spaces at higher Na and/or K content. The reduced basal spacings generally found
405 for the samples synthesised with 0.1 M alkali hydroxide solutions relative to the water
406 synthesised specimens can be attributed in part to exchange of interlayer Ca^{2+} with K^+ and/or
407 Na^+ (hydrated ionic radii of $Ca^{2+} = 4.12$ Å, $K^+ = 3.31$ Å and $Na^+ = 3.58$ Å⁶⁴). The
408 comparatively large differences in basal spacings between these samples indicate that other
409 factors, *e.g.* variations in the adsorbed interlayer water content, layer stacking configuration
410 and chain lengths of the C-(N,K-)A-S-H phases formed,⁵⁹ are also likely to be important.

411

412 A clear relationship between $d_{(002)}$ and Al content is not observed in Figure 6. However, basal
413 spacings for Al-containing C-(N,K-)A-S-H were measured to be 2-3 Å greater than their Al-
414 free counterparts at 20°C,^{60, 62} in contrast with these results. A clear trend in $d_{(002)}$ as a
415 function of the bulk alkali concentration is only identifiable at $Ca/Si^* = 0.6$ for the Al-
416 containing samples; the largest basal spacing is identified in the sample synthesised with 0.5
417 M NaOH/0.5 M KOH ($d_{(002)} = 16.1$ Å). This increase in basal spacing is again explained by
418 higher concentrations of alkali species in C-(N,K-)A-S-H interlayers at higher alkali content.

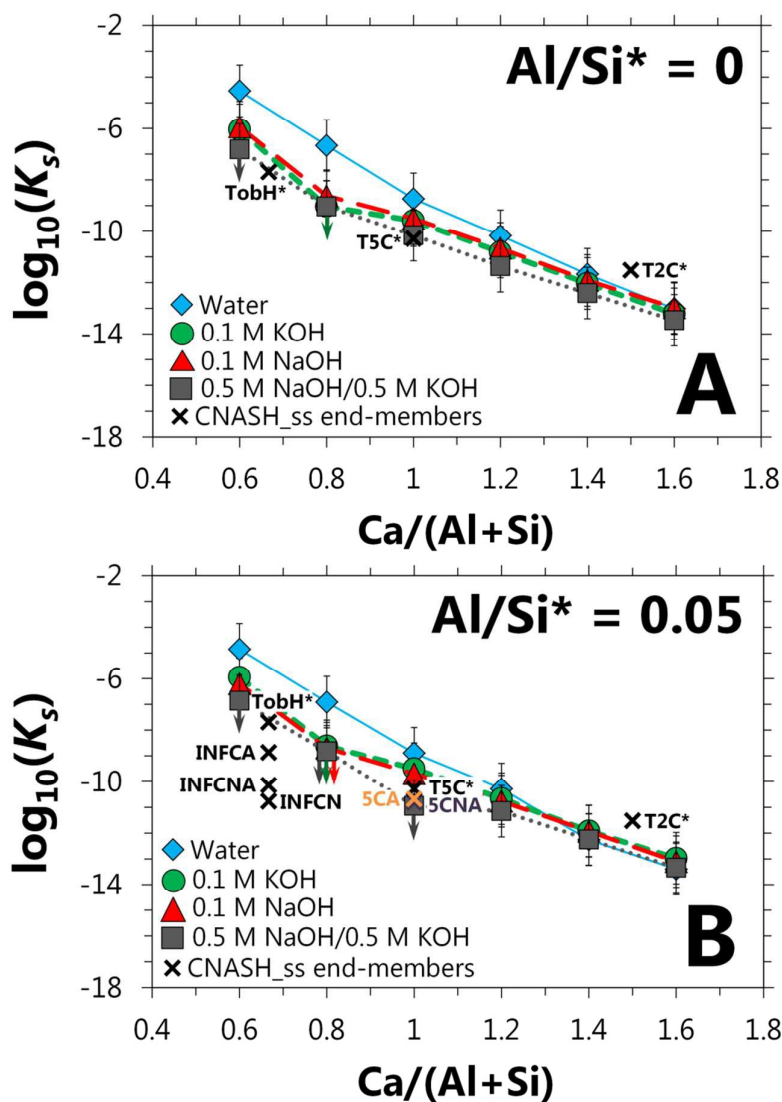
419

420 3.4 C-(N,K-)A-S-H solubility

421

422 Solubility products are calculated using eqs.(5-6) for C-(N,K-)A-S-H with hypothetical
423 chemical compositions of $\text{Ca}/(\text{Al}+\text{Si}) = 0.6, 0.8, 1, 1.2, 1.4$ and 1.6 , $\text{Al}/\text{Si} = 0$ and 0.05 ,
424 $\text{Na}/(\text{Al}+\text{Si}) = 0.2$ for samples containing Na, $\text{K}/(\text{Al}+\text{Si}) = 0.2$ for samples containing K,
425 $\text{H}_2\text{O}/\text{Si} = 1.2$, and $1 \text{ mol Al} + \text{Si}$, and shown in Figure 7. These $\text{Na}/(\text{Al}+\text{Si})$ and $\text{K}/(\text{Al}+\text{Si})$
426 ratios were chosen to approximate the alkali contents of the experimental C-(N,K-)A-S-H
427 products (Tables 1 and 2). Hypothetical chemical compositions were chosen to enable a more
428 direct comparison of the calculated solubility products as a function of Na, K and Al content.
429 Solubility products for C-(N,K-)A-S-H with chemical compositions determined by mass
430 balances from the XRD (Figure 2), IC and pH measurements (Figure 3), and TGA and
431 Rietveld analysis (Appendices S3 and S4, Electronic Supporting Information), are shown in
432 Appendix S6 (Electronic Supporting Information).

433



434

435

436

437

438

439

440

441

442

443

444

Figure 7. Solubility products (K_s) for hypothetical C-(N,K-)A-S-H phases with chemical compositions of A) $\text{Al/Si} = 0$ or B) $\text{Al/Si} = 0.05$, $\text{Na}/(\text{Al}+\text{Si}) = 0.2$ for the Na-containing systems, $\text{K}/(\text{Al}+\text{Si}) = 0.2$ for the K-containing systems, $\text{H}_2\text{O}/\text{Si} = 1.2$, and normalised to 1 mol Al + Si at 50°C . The estimated uncertainty depicted as error bars is ± 1 unit in the $\log_{10}(K_s)$ values, except for the points with downward-pointing arrows, which additionally represent maximum solubility product values as described in the text. The small crosses are solubility products for end-members of the CNASH_{ss} thermodynamic model²⁸ at 50°C . $\text{Al/Si}^* = \text{bulk Al/Si}$. Lines are for eye-guides only.

445

445 Figure 7 shows similar values and trends in the solubility products for both the Al-free and

446 Al-containing C-(N,K-)A-S-H end-members, *i.e.*, the results of this study indicate that this

447 phase is not greatly stabilised by the incorporation of Al. This is consistent with recently

448 published results for C-(A-)S-H synthesised with $\text{Ca/Si}^* = 1$ and cured at $7\text{-}80^\circ\text{C}$,¹⁴ where the

449 measured solubility of this phase did not change greatly between Al/Si* ratios of 0 and 0.15.
450 The downward-pointing arrows in Figure 7 for the Ca/Si* = 0.6 and 1 C-(N,K-)A-S-H
451 samples synthesised with 0.5 M NaOH/0.5 M KOH, and the Ca/Si* = 0.8 samples
452 synthesised with alkali hydroxide solutions, indicate that the calculated solubility products
453 are considered to be upper bounds; supernatant Ca concentrations were below the detection
454 limit for these samples, so an upper limit of [Ca] = 0.004 mM was chosen. Dissolved Al
455 concentrations were also below the detection limit for some samples (*e.g.* the Ca/Si* = 1.2,
456 Al/Si* = 0.05 sample synthesised with water, Figure 3), so [Al] = 0.003 mM was chosen for
457 these samples. The low Al content of the C-(N,K-)A-S-H products (Al/Si ~ 0.05) means that
458 the associated level of uncertainty in the K_s values for samples with [Al] below the detection
459 limit is lower than for the samples with [Ca] below the detection limit; downward pointing
460 arrows are only shown for the latter case in Figure 7.

461

462 The lower solubility products calculated for C-(N,K-)A-S-H with higher Ca/(Al+Si) ratios in
463 Figure 7 reflect the increased amounts of Ca included in the stoichiometric formulae for C-
464 (N,K-)A-S-H in these calculations at higher Ca/(Al+Si) ratios (Figure 7 shows solubility
465 products for C-(N,K-)A-S-H with chemical compositions normalised to one mole Al + Si),
466 but could additionally indicate that C-(N,K-)A-S-H is stabilised at higher Ca content within
467 the composition range analysed here. The solubility products of the C-(N,K-)A-S-H phases
468 synthesised using 0.1 M alkali hydroxide solutions are similar irrespective of the alkali
469 element used, indicating that both Na- and K-bearing C-(N,K-)A-S-H can be expected to
470 form in hydrated cements with non-zero concentrations of these alkali elements. Figure 7 also
471 shows that C-(N,K-)A-S-H solubility generally decreases slightly as the bulk alkali hydroxide
472 concentration is increased, but this finding is only significant for some C-(N,K-)A-S-H
473 phases with Ca/Si \leq 1. Similar trends of decreasing solubility with increasing alkali content

474 are also identified in solubility product calculations for hypothetical C-(N,K-)A-S-H phases
475 with $(\text{Na}+\text{K})/(\text{Al}+\text{Si}) = 0$ and $\text{Ca}/\text{Si} \leq 1$, which suggests that the structure of this phase may
476 be stabilised slightly as the bulk alkali concentration is increased. This will be discussed
477 further in section 3.5.

478

479 The end-members of the CNASH_{ss} thermodynamic model (Figure 7)²⁸ show the same
480 trends in C-(N,K-)A-S-H solubility as identified experimentally here. The reduced solubilities
481 of the Na-bearing end-members in the CNASH_{ss} thermodynamic model compared to the
482 experimental results are also consistent with their much higher Na content ($0.4 \leq \text{Na}/(\text{Al}+\text{Si})$
483 ≤ 0.46). The solubility product of the T2C* model end-member is consistent with the
484 experimental results, although the lower solubilities of the model T5C*, TobH* and INFCA
485 end-members relative to the experimental data indicates that their thermodynamic properties
486 should be adjusted slightly for simulations at 50°C to improve the temperature-dependent
487 behaviour of CNASH_{ss}.

488

489 The same method of analysis presented in sections 3.1-3.4 and shown in Figure 7 was applied
490 to C-(N,K-)A-S-H samples with $\text{Ca}/\text{Si}^* = 1$, $\text{Al}/\text{Si}^* = 0$ and 0.1, and synthesised with water,
491 0.5 NaOH and 0.5 M NaOH/0.5 M KOH solutions. The solid and liquid phase analyses for
492 these samples are presented in Appendix S7, Electronic Supporting Information, and the
493 resulting K_s values are shown in Table 3. These data show similar trends to those described
494 for Figure 7, *i.e.* a slight decrease in solubility as a function of increasing alkali hydroxide
495 concentration and no significant change in solubility as a function of the Al/Si^* ratio. These
496 results are discussed in terms of solubility-composition-structure relationships in C-(N,K-)A-
497 S-H, using the ²⁹Si MAS NMR analysis presented for these samples, in sections 3.5-3.6
498 below.

499 Table 3. Solubility products (K_s) for hypothetical C-(N,K-)A-S-H phases with chemical
 500 compositions of $\text{Ca}/(\text{Al}+\text{Si}) = 1$, Al/Si ratios = 0 ($\text{Al}/\text{Si}^* = 0$) or 0.1 ($\text{Al}/\text{Si}^* = 0.1$),
 501 $\text{Na}/(\text{Al}+\text{Si}) = 0.2$ for the Na-containing systems, $\text{K}/(\text{Al}+\text{Si}) = 0.2$ for the K-containing
 502 systems, $\text{H}_2\text{O}/\text{Si} = 1.2$, and normalised to 1 mol Al + Si at 50°C. The estimated uncertainty is
 503 ± 1 unit in $\log_{10}(K_s)$ values.

Al/Si* = 0	
Water	-8.7
0.5 M NaOH	-9.8
0.5 M NaOH/0.5 M KOH	-10.2
Al/Si* = 0.1	
Water	-8.9
0.5 M NaOH	-10.0
0.5 M NaOH/0.5 M KOH	$\leq -11.0^a$

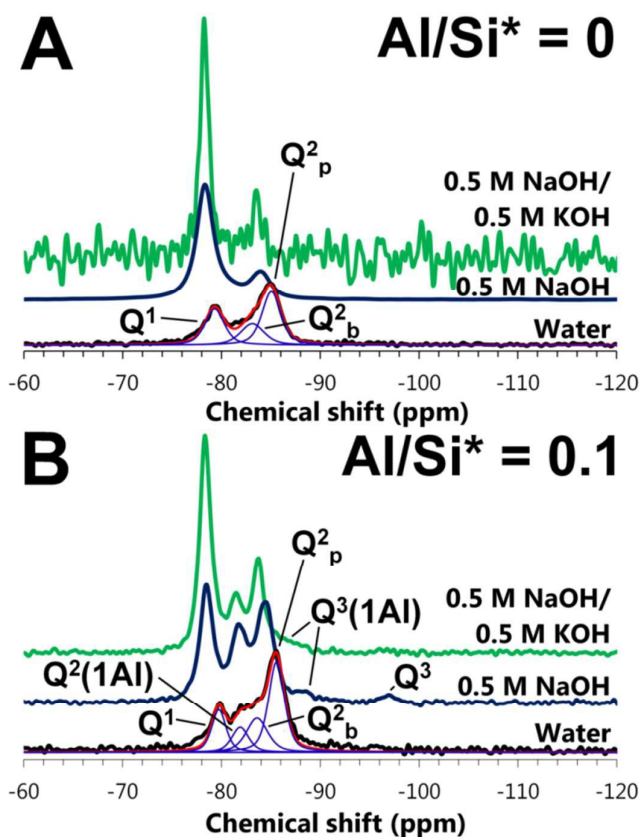
504 ^a Maximum values. Activities of Ca^{2+} , SiO_3^{2-} , AlO_2^- , Na^+ , K^+ , OH^- and H_2O were calculated
 505 using $[\text{Ca}] = 0.004$ mM, as the measured Ca concentration in the supernatant of this sample
 506 was below the detection limit.
 507

508 3.5 ²⁹Si MAS NMR

509

510 The ²⁹Si MAS NMR spectra of the C-(N,K-)S-H samples ($\text{Al}/\text{Si}^* = 0$) contain three
 511 resonances, that are assigned to chain-end sites (Q^1), bridging sites (Q^2_b) and paired sites
 512 (Q^2_p) (Figure 8A) respectively. In the spectra of the water-synthesised samples, these
 513 resonances are described by peaks located at isotropic chemical shifts (δ_{iso}) of -79.3 ppm, -
 514 83.1 ppm and -85.1 ppm respectively. Similar δ_{iso} values have been reported for alkali- and
 515 Al-free C-S-H aged at 40°C.^{65, 66} The spectrum for the Al-free sample synthesised with 0.5 M
 516 NaOH contains the same peaks but shifted by +1 to +2 ppm, which indicates that silanol
 517 groups in the 0.5 M NaOH sample are on average charge-balanced by less positively-charged
 518 species (*i.e.* Na^+ and/or H^+ rather than Ca^{2+}) relative to the alkali-free specimen.⁶⁷
 519 Comparable differences in δ_{iso} have also been reported between the Q^1 , Q^2_b and Q^2_p sites in
 520 C-(N,K-)S-H synthesised at different alkali concentrations.^{8, 9} The relative intensities of the
 521 Q^1 peaks are greatly increased in the presence of NaOH and KOH, which is discussed further
 522 in the context of a reduction in mean chain length (MCL) in section 3.6 below.

523



524

525

526 Figure 8. Solid-state ^{29}Si MAS NMR spectra of A) C-(N,K-)S-H ($\text{Al/Si}^* = 0$) and B) C-(N,K-)
 527 A-S-H ($\text{Al/Si}^* = 0.1$) samples, synthesised with $\text{Ca/Si}^* = 1$ and equilibrated at 50°C . The fits
 528 and deconvoluted peaks for the spectra of the water-synthesised samples are shown as red
 529 and blue lines respectively. Deconvolutions for each spectrum are shown in Appendix S8
 530 (Electronic Supporting Information). The relatively high level of noise in the spectrum of the
 531 $\text{Al/Si}^* = 0$ sample synthesised with 0.5 M NaOH/0.5 M KOH is caused by the very rapid
 532 relaxation of this sample. $\text{Al/Si}^* = \text{bulk Al/Si}$.

533

534 ^{29}Si resonances assigned to Q^1 , Q^2_{b} and Q^2_{p} sites are also identified in the spectra of the C-
 535 (N,K-)A-S-H ($\text{Al/Si}^* = 0.1$) samples (Figure 8B). These spectra also contain an additional
 536 resonance assigned to Si in paired sites bonded to structurally-incorporated Al in bridging
 537 sites (i.e. $\text{Q}^2(1\text{Al})$) in C-A-S-H, located at $\delta_{\text{iso}} = -82$ ppm in the spectrum for the alkali-free
 538 sample. $\text{Q}^2(1\text{Al})$ sites identified in laboratory-synthesised C-A-S-H samples equilibrated at
 539 23°C are located at similar δ_{iso} values.⁶⁸

540

541 Peaks assigned to Q^1 , Q^2_{b} , Q^2_{p} and $\text{Q}^2(1\text{Al})$ are shifted by +0.4 to +1 ppm in the spectrum for
 542 the Al-containing sample synthesised with 0.5 M NaOH relative to the alkali-free C-A-S-H

543 sample (Figure 8B), which is consistent with ^{29}Si MAS NMR spectra of laboratory-
544 synthesised C-(N,K-)A-S-H produced at 20-25°C.^{8, 9} The intensity of the Q^1 peak is also
545 much greater in the presence of Na and/or K in this sample, similar to the spectra for Al-free
546 C-(N,K-)S-H (Figure 8A). Additional $Q^3(1\text{Al})$ and Q^3 resonances at -88.6 and -96.8 ppm are
547 observed in the spectrum of the 0.5 M NaOH sample, indicating the formation of a cross-
548 linked C-(N,K-)A-S-H product. The δ_{iso} value of the Q^3 site is equivalent to the chemical shift
549 of this site in laboratory-synthesised C-A-S-H equilibrated at 80°C¹⁴ and in Al-tobermorite
550 formed in 2000-year old Roman seawater concrete,³¹ and is similar to the chemical shift of
551 this site in (Al-)tobermorites synthesised at 150°C⁶⁹ and 175°C.^{70, 71} However, the δ_{iso} value
552 of the $Q^3(1\text{Al})$ site is shifted by approximately +3 ppm relative to the chemical shift of this
553 site in the aforementioned literature; this is again attributed to the association of a greater
554 proportion of less positively-charged dissolved species (*e.g.* Na^+ rather than Ca^{2+}) with Si
555 atoms in $Q^3(1\text{Al})$ sites, resulting from the much higher alkali concentrations used here.

556

557 Each component peak is shifted to a slightly more positive δ_{iso} value by further increasing the
558 alkali hydroxide concentrations of the synthesis solutions to 1 M (Figure 8B, sample 0.5 M
559 NaOH/0.5 M KOH), suggesting additional uptake of $\text{Na}^+/\text{K}^+/\text{H}^+$ in C-(N,K-)A-S-H
560 interlayers, while the Q^3 site is no longer identified. The disappearance of the Q^3 site at a bulk
561 alkali concentration of 1 M, and the presence of $Q^3(1\text{Al})$ resonances at -87 to -89 ppm in the
562 Al and alkali-containing samples, are consistent with the features of ^{29}Si MAS NMR spectra
563 of Na_2CO_3 and Na_2SiO_3 -activated slag cement pastes cured under ambient conditions,^{5, 72}
564 where $Q^3(1\text{Al})$ -containing cross-linked C-(N,K-)A-S-H products are sometimes present in
565 this chemical shift range. The identification of Q^3 -type sites in the C-(N,K-)A-S-H samples
566 equilibrated at 50°C here, rather than the higher temperatures needed to form these structures
567 in C-A-S-H specimens synthesised with Al but without alkali,¹⁴ shows that the formation of -

568 Al-O-Si- cross-links in C-(N,K-)A-S-H products is greatly promoted at higher alkali content.
 569 The intensity of the Q¹ peaks are further increased by increasing the alkali hydroxide
 570 concentration to 1 M.

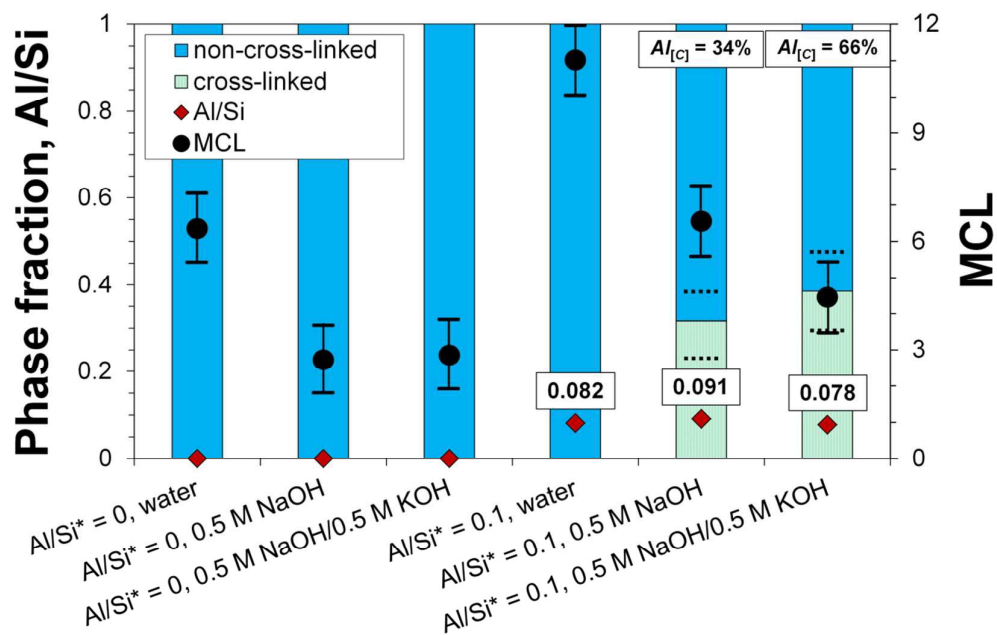
571

572 3.6 Structural models and implications

573

574 Al/Si ratios, MCLs and cross-linked phase fractions for the C-(N,K-)A-S-H products (Figure
 575 9) are calculated using the ²⁹Si MAS NMR spectral deconvolution results (Figure 8 and
 576 Appendix S8, Electronic Supporting Information) and the ‘Cross-linked Substituted
 577 Tobermorite Model’ (CSTM),³⁷ by representing this phase as a mixture of cross-linked and
 578 non-cross-linked tobermorite-like components.

579



580

581

582

583

584

585

586

587

588

Figure 9. C-(N,K-)S-H and C-(N,K-)A-S-H structural parameters calculated from deconvolution analysis of the ²⁹Si MAS NMR spectra (Figure 8), determined using the ‘Cross-linked Substituted Tobermorite Model’ (CSTM)³⁷ for mixed cross-linked/non-cross-linked tobermorite-like phases. The expected error bounds of the deconvolution results are represented by symbol size for the Al/Si ratios, by dotted black lines for the cross-linked phase fractions and by error bars for the MCL values. Al_[C] = percentage of Al in cross-linked C-(N,K-)A-S-H (eq.(1)). Al/Si* = bulk Al/Si.

589 The results obtained by applying the CSTM³⁷ to the ²⁹Si MAS NMR spectral deconvolutions
590 show that the MCLs of the C-(N,K-)A-S-H products decrease with increasing alkali
591 concentration, due mainly to the much greater prevalence of Q¹ sites in the presence of Na
592 and/or K (Figure 8). The calculated MCLs are also lower in the systems containing less Al.
593 The calculated Al/Si ratios are similar to the Al/Si* ratios used in synthesis (Al/Si* = 0.1),
594 with the small differences explained by the formation of small amounts of C₃AH₆/Al(OH)₃ in
595 the alkali-free and 0.5 M NaOH/0.5 M KOH samples, and C₄AcH₁₁/C₃AH₆/Al(OH)₃ in the
596 0.5 M NaOH sample (Appendix S7, Electronic Supporting Information).¹⁴ The alkali and Al-
597 containing C-(N,K-)A-S-H products show similar levels of cross-linking, although the
598 percentage of Al in the cross-linked components ($Al_{[C]}$) of this phase is higher in the sample
599 synthesised using 0.5 M NaOH/0.5 M KOH (66%) relative to the sample synthesised with 0.5
600 M NaOH (34%).

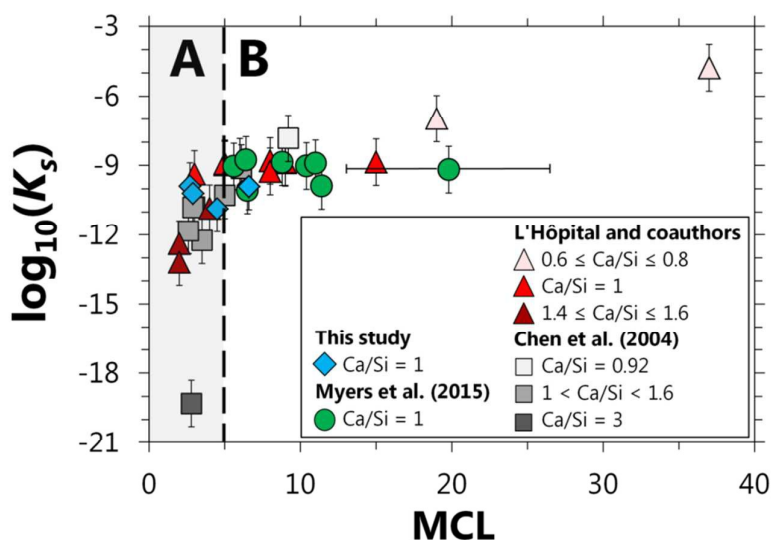
601

602 The calculated $Al_{[C]}$ values (Figure 9) show that the uptake of Al into cross-linked C-(N,K-
603)A-S-H components is enhanced as the bulk alkali hydroxide concentration is increased, but
604 also that there is not an extremely strong preference for partitioning of Al into either one of
605 the two structural types. This view is supported by recent work on the role of Al in cross-
606 linking of C-(N,K-)A-S-H in Na₂SiO₃-activated slag cements cured for 1-180 days at room
607 temperature, which reported $Al_{[C]}$ values of 40-60%.⁷²

608

609 The key alkali-dependent structural changes are therefore: reduced MCL (Figure 9);
610 increased basal spacings at Ca/Si* ratios < 1 (Figure 6); and increased cross-linking and $Al_{[C]}$
611 (in the presence of Al, Figure 9) at higher alkali hydroxide concentrations. A comparison of
612 these structural changes with the slightly reduced C-(N,K-)A-S-H solubilities determined at
613 higher alkali hydroxide concentration and Ca/(Al+Si) ratios ≤ 1 (section 3.4) suggests that the

614 solubility and MCL of this phase may be directly related in this range of Ca/(Al+Si) ratios.
 615 The influence of Ca composition on C-(N,K-)A-S-H solubility dominates at higher
 616 Ca/(Al+Si) ratios, *i.e.* at low MCL values, demonstrated by large reductions in the solubility
 617 of this phase as a function of increasing Ca/(Al+Si) ratio at the limit $MCL \rightarrow 2$ (region A in
 618 Figure 10). The Ca/(Al+Si) ratios obtained by mass balance and marked in the legend in
 619 Figure 10 reflect the total amount of Ca in C-(N,K-)A-S-H; this parameter does not
 620 distinguish between Ca present as charge-balancing cations in the interlayer or adsorbed on
 621 external surfaces, or structurally-bound in Ca-O sheets (Figure 1), whereas the MCL
 622 parameter describes the structure of the (alumino)silicate chains and Ca-O sheets only.
 623

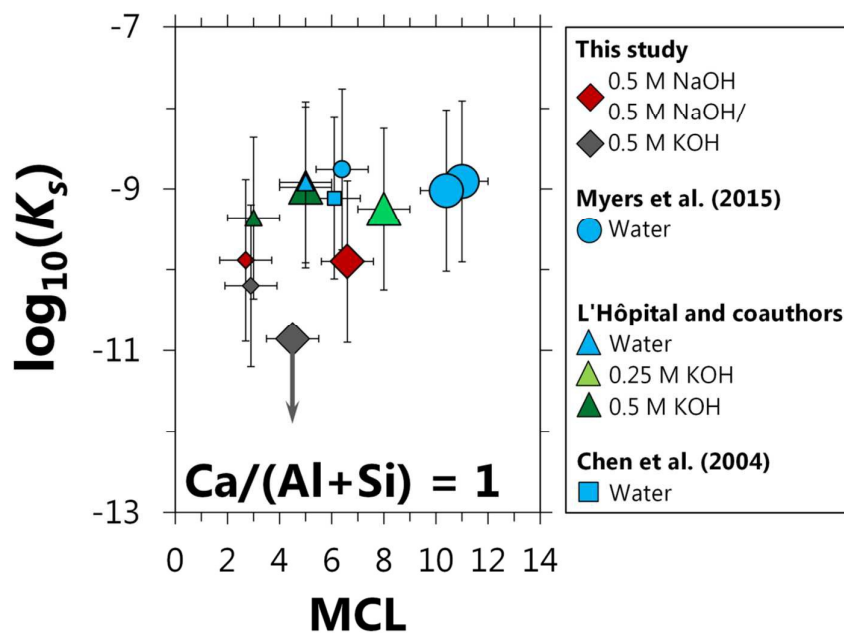


624
 625 Figure 10. Solubility products for C-(N,K-)A-S-H plotted as a function of MCL, calculated
 626 using the dissolution reaction shown in eq.(5) with regions: A) describing C-(N,K-)A-S-H
 627 with highly variable Ca/(Al+Si) ratios and slightly variable MCL; and B) describing C-(N,K-
 628)A-S-H with variable Ca/(Al+Si) and MCL. The references for the symbols used are: blue
 629 diamonds, this study; green circles, C-(A-)S-H equilibrated at 7-80°C in ¹⁴; red triangles, C-
 630 (N,K-)A-S-H equilibrated at 20°C in ^{8,60}; and grey squares, C-S-H equilibrated at 22°C in ⁷³.
 631 Solubility products are calculated using H₂O/Si = 1.2 and Ca/Si ratios taken directly from the
 632 literature for the data in ⁷³, or specified to have a total of 1 mole Si + Al with Ca/Si and Al/Si
 633 ratios equivalent to the bulk Ca-Al-Si compositions used, Na/Si ratios = 0.2 for the Na-
 634 containing phases, K/Si ratios = 0.2 for the K-containing phases and H₂O/Si ratios = 1.2 for
 635 the data in ^{8,14,60} and in this study. The expected experimental uncertainty is represented by
 636 error bars, or by the size of the symbols used in the absence of horizontal error bars for MCL
 637 values.

638

639 The effects of MCL and $\text{Ca}/(\text{Al}+\text{Si})$ ratio on C-(N,K-)A-S-H solubility cannot be
 640 distinguished from one another in region B of Figure 10 because C-(N,K-)A-S-H can contain
 641 many different total $\text{Ca}/(\text{Al}+\text{Si})$ ratios at a fixed MCL value, for $\text{MCL} > 5$.⁵⁹ Therefore,
 642 selected solubility data for C-(N,K-)A-S-H with $\text{Ca}/(\text{Al}+\text{Si}) = 1$ were plotted as a function of
 643 MCL in Figure 11.

644



645

646 Figure 11. Solubility products for C-(N,K-)A-S-H plotted as a function of the MCL,
 647 calculated using the dissolution reaction shown in eq.(5) at a $\text{Ca}/(\text{Al}+\text{Si})$ ratio = 1. The
 648 references for the symbols used are: diamonds, this study ($\text{Ca}/\text{Si}^* = 1$); circles, C-(A-)S-H
 649 synthesised with $\text{Ca}/\text{Si}^* = 1$ and equilibrated at 20-50°C in¹⁴; triangles, C-(N,K-)A-S-H
 650 synthesised with $\text{Ca}/\text{Si}^* = 1$ and equilibrated at 20°C in^{8,60}; and square, C-S-H equilibrated
 651 at 22°C with $\text{Ca}/\text{Si} = 1.03$ in⁷³. Large symbols are data at $\text{Al}/\text{Si}^* = 0.1$ and small symbols are
 652 data at $\text{Al}/\text{Si}^* = 0$. C-(N,K-)A-S-H solubility products are calculated using $\text{H}_2\text{O}/\text{Si} = 1.2$ and
 653 Ca/Si ratios taken directly from the literature for the datum in⁷³, or specified to have a total
 654 of 1 mole Si + Al with Ca/Si and Al/Si^* ratios equivalent to the bulk Ca-Al-Si compositions
 655 used, Na/Si ratios = 0.2 for the Na-containing phases, K/Si ratios = 0.2 for the K-containing
 656 phases and $\text{H}_2\text{O}/\text{Si}$ ratios = 1.2 for the data in^{8,14,60} and in this study. Error bars represent the
 657 expected experimental uncertainty except for the point with a downward-pointing arrow,
 658 which additionally represents a maximum solubility product value, as described in the text for
 659 Figure 7.

660

661 Figure 11 shows an inverse correlation between MCL and the bulk alkali hydroxide
662 concentration, in good agreement with the ^{29}Si MAS NMR results presented in Figure 9, and
663 also slightly reduced C-(N,K-)A-S-H solubility products in samples synthesised with more
664 highly concentrated alkali hydroxide solutions, consistent with the trends in C-(N,K-)A-S-H
665 solubility shown in Figure 7 at $\text{Ca}/(\text{Al}+\text{Si}) = 1$. However, Figure 11 does not show a
666 significant difference in C-(N,K-)A-S-H solubility as a function of Al content, despite the
667 longer chain lengths of the Al-containing C-(N,K-)A-S-H phases compared to their Al-free
668 counterparts. Therefore, these results indicate that the MCL structural parameter does not
669 play a key role in influencing the solubility of C-(N,K-)A-S-H at a $\text{Ca}/(\text{Al}+\text{Si})$ ratio = 1. This
670 analysis is consistent with recently reported results for C-(A-)S-H that showed comparable
671 solubility products for this phase independent of the Al content.¹⁴

672

673 Alternative factors that could account for the slightly stabilised C-(N,K-)A-S-H structures
674 identified here at increased bulk alkali hydroxide concentrations and $\text{Ca}/(\text{Al}+\text{Si})$ ratios ≤ 1
675 (Figure 7) would then need to be proposed: increased cross-linking (Figure 9) or changes to
676 the nanoparticulate layered structure of this phase (Figure 6 and ⁵⁹) could be potential
677 candidates. However, the large uncertainty ($\pm 1 \log_{10}$ unit) of the solubility products calculated
678 here (Figure 7) and the limited availability of solubility data for C-(N,K-)A-S-H at
679 $\text{Ca}/(\text{Al}+\text{Si})$ ratios < 1 mean that these proposed structure-solubility relationships cannot be
680 considered fully conclusive. Further work clarifying the role of structure on the solubility of
681 C-(N,K-)A-S-H would be greatly beneficial in further enabling the design of chemically-
682 stable and durable cementitious binders based on engineering controls such as the mix design
683 and curing temperature.

684

685 **4. Conclusions**

686

687 The effect of alkali, Al and Ca on the structure and solubility of C-(N,K-)A-S-H equilibrated
688 at 50°C was investigated in this paper. In general, similar composition-solubility-structure
689 trends are observed at 20°C to those identified here. The long-range order of the alkali-
690 containing C-(N,K-)A-S-H products was much greater than in those synthesised in the
691 absence of alkalis. C-(N,K-)A-S-H basal spacings were generally greater at lower Ca content
692 and at higher alkali concentrations in the samples synthesised using alkaline hydroxide
693 solutions; this latter factor was attributed to the uptake of additional Na⁺/K⁺ species in C-
694 (N,K-)A-S-H interlayers. However, no clear trend in basal spacing as a function of Al content
695 was identified here, in contrast to results reported for this phase at 20°C.

696

697 The concentrations of Ca decreased and the concentrations of Si and Al increased in the
698 supernatants as functions of increasing alkali hydroxide concentration. More alkali was
699 incorporated in C-(N,K-)A-S-H synthesised with lower Ca and higher alkali hydroxide
700 concentrations. Alkali uptake in this phase was found to be independent, within the
701 experimental uncertainty, of the alkali type (Na or K) and Al/Si ratio at the relatively low
702 amounts of Al added to each sample (bulk Al/Si ≤ 0.05).

703

704 Shorter mean chain lengths, increased cross-linking, and incorporation of more Al into cross-
705 linked C-(N,K-)A-S-H components were identified upon increasing the bulk alkali and Al
706 content. Mixed cross-linked/non-cross-linked C-(N,K-)A-S-H was only formed in the
707 presence of both alkali and Al. A reduction in C-(N,K-)A-S-H solubility was found at higher
708 bulk alkali hydroxide concentrations, but this result was only significant for some samples
709 prepared with bulk Ca/Si ratios ≤ 1. The stability of this phase did not vary greatly as a

710 function of the Al/Si ratio. The reduced C-(N,K-)A-S-H solubility calculated at higher alkali
711 content was discussed to be partly related to structural changes in this phase, and it was
712 tentatively proposed that the MCL does not play a key role in these solubility-structure
713 relationships. These results provide new insight into the composition-structure-solubility
714 relationships in C-(N,K-)A-S-H, which will improve how hydrated alkali and Al-containing
715 cements are understood to perform in service.

716

717 **5. Supporting information**

718

719 Electronic Supplementary Information (ESI) available: Appendix S1 contains the details of
720 the structural constraints used to deconvolute the ^{29}Si MAS NMR spectra; the thermodynamic
721 database used is presented in Appendix S2; tabulated phase quantification results from XRD,
722 TGA and Rietveld analysis are provided in Appendix S3; TGA results are shown in Appendix
723 S4; saturation indices calculated from the measured supernatant concentrations are shown in
724 Appendix S5; tabulated supernatant concentrations and the solubility products for C-(N,K-
725)A-S-H with chemical compositions determined by mass balance are provided in Appendix
726 S6; additional solid and liquid phase data for the Al/Si* = 0 and 0.1 C-(N,K-)A-S-H samples
727 studied by ^{29}Si MAS NMR are presented in Appendix S7; and detailed ^{29}Si MAS NMR
728 spectral deconvolution results are provided in Appendix S8.

729

730 **6. Acknowledgements**

731

732 The authors thank Salaheddine Alahrache and Daniel Rentsch for assistance with NMR
733 spectroscopy, Boris Ingold for assistance with XRD, Ellina Bernard, Boris Ingold and
734 Nikolajs Toropovs for assistance with TGA, and the Swiss National Science Foundation grant

735 n° 130419 for the financial support of E. L'Hôpital. The NMR hardware was partially granted
736 by the Swiss National Science Foundation (grant 206021_150638/1).

737

738 **7. References**

739

- 740 1. H. F. W. Taylor, *Cement Chemistry*, Thomas Telford Publishing, London, 1997.
- 741 2. A. Fernández-Jiménez and A. Palomo, *Fuel*, 2003, **82**, 2259-2265.
- 742 3. J. L. Provis and S. A. Bernal, *Annu. Rev. Mater. Res.*, 2014, **44**, 299-327.
- 743 4. R. Snellings, *J. Am. Ceram. Soc.*, 2013, **96**, 2467-2475.
- 744 5. S. A. Bernal, J. L. Provis, R. J. Myers, R. San Nicolas and J. S. J. van Deventer,
745 *Mater. Struct.*, 2015, **48**, 517-529.
- 746 6. T. Chappex and K. Scrivener, *Cem. Concr. Res.*, 2012, **42**, 1049-1054.
- 747 7. A. Leemann, G. Le Saout, F. Winnefeld, D. Rentsch and B. Lothenbach, *J. Am.*
748 *Ceram. Soc.*, 2011, **94**, 1243-1249.
- 749 8. E. L'Hôpital, B. Lothenbach, G. Le Saoût, D. A. Kulik and K. Scrivener, *Cem. Concr.*
750 *Res.*, submitted.
- 751 9. I. Lognot, I. Klur and A. Nonat, in *Nuclear magnetic resonance spectroscopy of*
752 *cement-based materials*, eds. P. Colombet, H. Zanni, A.-R. Grimmer and P. Sozzani,
753 Springer, Berlin, 1998, ch. 13, pp. 189-196.
- 754 10. J. Duchesne and E. J. Reardon, *Cem. Concr. Res.*, 1995, **25**, 1043-1053.
- 755 11. T. T. H. Bach, E. Chabas, I. Pochard, C. Cau-dit-Coumes, J. Haas, F. Frizon and A.
756 Nonat, *Cem. Concr. Res.*, 2013, **51**, 14-21.
- 757 12. I. G. Richardson and G. W. Groves, *J. Mater. Sci.*, 1993, **28**, 265-277.
- 758 13. I. G. Richardson, *Cem. Concr. Res.*, 2008, **38**, 137-158.

- 759 14. R. J. Myers, E. L'Hôpital, J. L. Provis and B. Lothenbach, *Cem. Concr. Res.*, 2015, **68**,
760 83-93.
- 761 15. L. Pegado, C. Labbez and S. V. Churakov, *J. Mater. Chem. A*, 2014, **2**, 3477-3483.
- 762 16. M. D. Andersen, H. J. Jakobsen and J. Skibsted, *Cem. Concr. Res.*, 2006, **36**, 3-17.
- 763 17. G. Renaudin, J. Russias, F. Leroux, C. Cau dit Coumes and F. Frizon, *J. Solid State*
764 *Chem.*, 2009, **182**, 3320-3329.
- 765 18. G. K. Sun, J. F. Young and R. J. Kirkpatrick, *Cem. Concr. Res.*, 2006, **36**, 18-29.
- 766 19. C. Labbez, I. Pochard, B. Jönsson and A. Nonat, *Cem. Concr. Res.*, 2011, **41**, 161-168.
- 767 20. E. Bonaccorsi, S. Merlino and A. R. Kampf, *J. Am. Ceram. Soc.*, 2005, **88**, 505-512.
- 768 21. S. Y. Hong and F. P. Glasser, *Cem. Concr. Res.*, 1999, **29**, 1893-1903.
- 769 22. D. E. Macphee, K. Luke, F. P. Glasser and E. E. Lachowski, *J. Am. Ceram. Soc.*,
770 1989, **72**, 646-654.
- 771 23. G. L. Kalousek, *J. Res. Natl. Bur. Stand.*, 1944, **32**, 285-302.
- 772 24. S. J. Way and A. Shayan, *Cem. Concr. Res.*, 1992, **22**, 915-926.
- 773 25. H. Stade, *Cem. Concr. Res.*, 1989, **19**, 802-810.
- 774 26. P. Nieto and H. Zanni, *J. Mater. Sci.*, 1997, **32**, 3419-3425.
- 775 27. B. Lothenbach, G. Le Saout, M. Ben Haha, R. Figi and E. Wieland, *Cem. Concr. Res.*,
776 2012, **42**, 410-423.
- 777 28. R. J. Myers, S. A. Bernal and J. L. Provis, *Cem. Concr. Res.*, 2014, **66**, 27-47.
- 778 29. B. Lothenbach, K. Scrivener and R. D. Hooton, *Cem. Concr. Res.*, 2011, **41**, 1244-
779 1256.
- 780 30. R. Taylor, I. G. Richardson and R. M. D. Brydson, *Cem. Concr. Res.*, 2010, **40**, 971-
781 983.

- 782 31. M. D. Jackson, S. R. Chae, S. R. Mulcahy, C. Meral, R. Taylor, P. Li, A.-H. Emwas, J.
783 Moon, S. Yoon, G. Vola, H.-R. Wenk and P. J. M. Monteiro, *Am. Mineral.*, 2013, **98**,
784 1669-1687.
- 785 32. H. Viallis, P. Faucon, J. C. Petit and A. Nonat, *J. Phys. Chem. B*, 1999, **103**, 5212-
786 5219.
- 787 33. J. Skibsted and M. D. Andersen, *J. Am. Ceram. Soc.*, 2013, **96**, 651-656.
- 788 34. S. Y. Hong and F. P. Glasser, *Cem. Concr. Res.*, 2002, **32**, 1101-1111.
- 789 35. E. L'Hôpital, B. Lothenbach, K. Scrivener and D. A. Kulik, *Cem. Concr. Res.*,
790 submitted.
- 791 36. B. H. O'Connor and M. D. Raven, *Powder Diffr.*, 1988, **3**, 2-6.
- 792 37. R. J. Myers, S. A. Bernal, R. San Nicolas and J. L. Provis, *Langmuir*, 2013, **29**, 5294-
793 5306.
- 794 38. D. A. Kulik, T. Wagner, S. V. Dmytrieva, G. Kosakowski, F. F. Hingerl, K. V.
795 Chudnenko and U. Berner, *Comput. Geosci.*, 2013, **17**, 1-24.
- 796 39. T. Wagner, D. A. Kulik, F. F. Hingerl and S. V. Dmytrieva, *Can. Mineral.*, 2012, **50**,
797 1173-1195.
- 798 40. T. Thoenen, W. Hummel and U. Berner, *Mineral. Mag.*, 2013, **77**, 2327.
- 799 41. W. Hummel, U. Berner, E. Curti, F. J. Pearson and T. Thoenen, *Nagra/PSI Chemical*
800 *Thermodynamic Database 01/01*, Universal Publishers, Parkland, Florida, 2002.
- 801 42. D. A. Kulik and M. Kersten, *J. Am. Ceram. Soc.*, 2001, **84**, 3017-3026.
- 802 43. B. Lothenbach, T. Matschei, G. Möschner and F. P. Glasser, *Cem. Concr. Res.*, 2008,
803 **38**, 1-18.
- 804 44. B. Lothenbach and F. Winnefeld, *Cem. Concr. Res.*, 2006, **36**, 209-226.
- 805 45. T. Matschei, B. Lothenbach and F. P. Glasser, *Cem. Concr. Res.*, 2007, **37**, 1379-1410.

- 806 46. G. Möschner, B. Lothenbach, J. Rose, A. Ulrich, R. Figi and R. Kretzschmar,
807 *Geochim. Cosmochim. Acta*, 2008, **72**, 1-18.
- 808 47. G. Möschner, B. Lothenbach, F. Winnefeld, A. Ulrich, R. Figi and R. Kretzschmar,
809 *Cem. Concr. Res.*, 2009, **39**, 482-489.
- 810 48. T. Schmidt, B. Lothenbach, M. Romer, K. Scrivener, D. Rentsch and R. Figi, *Cem.*
811 *Conc. Res.*, 2008, **38**, 337-349.
- 812 49. D. A. Kulik and M. Kersten, *Environ. Sci. Technol.*, 2002, **36**, 2926-2931.
- 813 50. B. Lothenbach, L. Pelletier-Chaignat and F. Winnefeld, *Cem. Concr. Res.*, 2012, **42**,
814 1621-1634.
- 815 51. B. Z. Dilnesa, B. Lothenbach, G. Renaudin, A. Wichser and D. Kulik, *Cem. Concr.*
816 *Res.*, 2014, **59**, 96-111.
- 817 52. H. C. Helgeson, D. H. Kirkham and G. C. Flowers, *Am. J. Sci.*, 1981, **281**, 1249-1516.
- 818 53. Y. Lee, Y. Lee and D. Seoung, *Am. Mineral.*, 2010, **95**, 1636-1641.
- 819 54. T. Runčevski, R. E. Dinnebier, O. V. Magdysyuk and H. Pöllmann, *Acta Crystallogr.*
820 *B*, 2012, **68**, 493-500.
- 821 55. P. Faucon, J. C. Petit, T. Charpentier, J. F. Jacquinet and F. Adenot, *J. Am. Ceram.*
822 *Soc.*, 1999, **82**, 1307-1312.
- 823 56. X. Pardal, I. Pochard and A. Nonat, *Cem. Concr. Res.*, 2009, **39**, 637-643.
- 824 57. H. M. Jennings, *Cem. Concr. Res.*, 2008, **38**, 275-289.
- 825 58. A. C. A. Muller, K. L. Scrivener, A. M. Gajewicz and P. J. McDonald, *Micropor.*
826 *Mesopor. Mat.*, 2013, **178**, 99-103.
- 827 59. I. Richardson, *Acta Crystallogr. B.*, 2014, **70**, 903-923.
- 828 60. E. L'Hôpital, Ph.D. Thesis, École Polytechnique Fédérale de Lausanne, 2014.
- 829 61. S. Grangeon, F. Claret, Y. Linard and C. Chiaberge, *Acta Crystallogr. B*, 2013, **69**,
830 465-473.

- 831 62. G. Renaudin, J. Russias, F. Leroux, F. Frizon and C. Cau dit Coumes, *J. Solid State*
832 *Chem.*, 2009, **182**, 3312-3319.
- 833 63. K. Garbev, G. Beuchle, M. Bornefeld, L. Black and P. Stemmermann, *J. Am. Ceram.*
834 *Soc.*, 2008, **91**, 3005-3014.
- 835 64. B. E. Conway, *Ionic hydration in chemistry and biophysics*, Elsevier Scientific,
836 Amsterdam, 1981.
- 837 65. X. Cong and R. J. Kirkpatrick, *Adv. Cem. Based Mater.*, 1996, **3**, 144-156.
- 838 66. F. Brunet, P. Bertani, T. Charpentier, A. Nonat and J. Virlet, *J. Phys. Chem. B*, 2004,
839 **108**, 15494-15502.
- 840 67. P. Rejmak, J. S. Dolado, M. J. Stott and A. Ayuela, *J. Phys. Chem. C*, 2012, **116**,
841 9755-9761.
- 842 68. X. Pardal, F. Brunet, T. Charpentier, I. Pochard and A. Nonat, *Inorg. Chem.*, 2012, **51**,
843 1827-1836.
- 844 69. J. Houston, R. Maxwell and S. Carroll, *Geochem. Trans.*, 2009, **10**, 1-14.
- 845 70. M. Tsuji, S. Komarneni and P. Malla, *J. Am. Ceram. Soc.*, 1991, **74**, 274-279.
- 846 71. X. Cong and R. J. Kirkpatrick, *Adv. Cem. Based Mater.*, 1996, **3**, 133-143.
- 847 72. R. J. Myers, S. A. Bernal, J. L. Provis, J. D. Gehman and J. S. J. van Deventer, *J. Am.*
848 *Ceram. Soc.*, 2015, **98**, 996-1004.
- 849 73. J. J. Chen, J. J. Thomas, H. F. W. Taylor and H. M. Jennings, *Cem. Concr. Res.*, 2004,
850 **34**, 1499-1519.
- 851
- 852

1

Table of contents entry

2 **Table of contents abstract**

3

4 Solubility-structure-composition relationships in calcium (alkali) aluminosilicate hydrate (C-

5 (N,K-)A-S-H) are analysed, including the mean chain length, basal spacing and cross-linking.

6

7 **Table of contents graphic**

8

